Article

Cancer Cell

# Combination of Hypoglycemia and Metformin Impairs Tumor Metabolic Plasticity and Growth by Modulating the PP2A-GSK3β-MCL-1 Axis

## Graphical Abstract

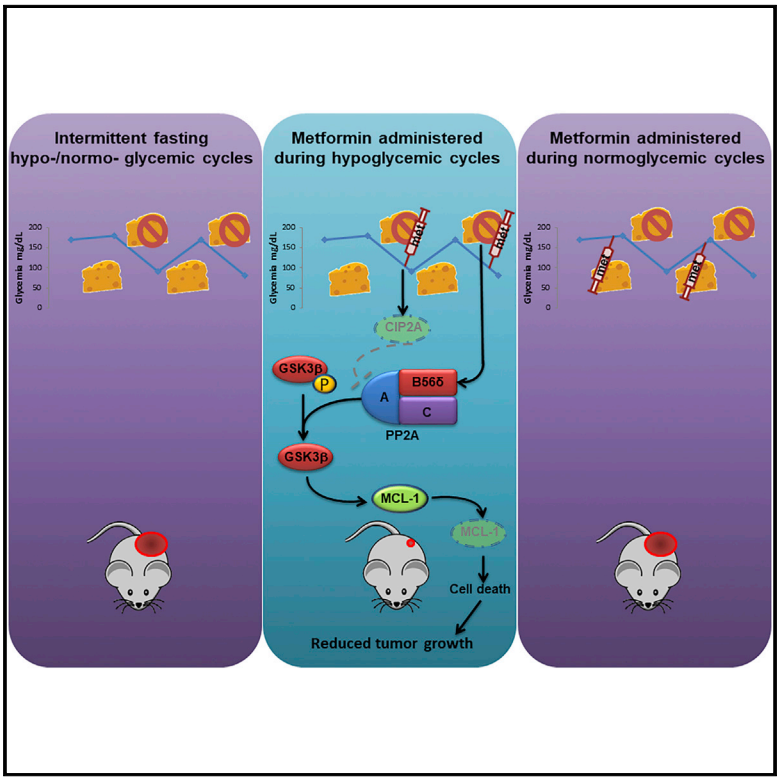


## Highlights

- Metformin plus fasting-induced hypoglycemia synergistically reduces tumor growth
- PP2A-GSK3β-MCL-1 axis mediates the synergistic cytotoxicity of the combination
- Simultaneous CIP2A inhibition and B56δ upregulation dictate combination specificity

## Authors

Mohamed Elgendy, Marco Cirò, Amir Hosseini, ..., Wolfram Weckwerth, Marco Foiani, Saverio Minucci

## Correspondence

mohamed.elgendy@univie.ac.at (M.E.), saverio.minucci@ieo.it (S.M.)

## In Brief

Elgendy et al. show that metformin administered during the fasting period synergizes with 24-h feeding/fasting cycles to suppress tumor growth. Inhibition of CIP2A by metformin and upregulation of B56δ by low glucose activates PP2A toward GSK3β leading to reduced pro-survival protein MCL-1 and cell death.

Elgendy et al., 2019, Cancer Cell *35*, 798–815
May 13, 2019 
https://doi.org/10.1016/j.ccell.2019.03.007

CellPress

CellPress

Cancer Cell
Article

# Combination of Hypoglycemia and Metformin Impairs Tumor Metabolic Plasticity and Growth by Modulating the PP2A-GSK3β-MCL-1 Axis

Mohamed Elgendy,[1,14,*] Marco Cirò,[2] Amir Hosseini,[1] Jakob Weiszmann,[3,12] Luca Mazzarella,[1] Elisa Ferrari,[2] Riccardo Cazzoli,[1] Giuseppe Curigliano,[4] Andrea DeCensi,[5] Bernardo Bonanni,[6] Alfredo Budillon,[7] Pier Giuseppe Pelicci,[1,8] Veerle Janssens,[9] Manfred Ogris,[10] Manuela Baccarini,[11] Luisa Lanfrancone,[1] Wolfram Weckwerth,[3,12] Marco Foiani,[2,8] and Saverio Minucci[1,13,15,*]

[1]Department of Experimental Oncology, IEO, European Institute of Oncology IRCCS, via Adamello 16, 20139 Milan, Italy
[2]Experimental Therapeutics Program, IFOM – The FIRC Institute for Molecular Oncology Foundation, Via Adamello 16, 20139 Milan, Italy
[3]Department of Ecogenomics and Systems Biology, Faculty of Sciences, University of Vienna, Vienna, Austria
[4]Division of Early Drug Development, IEO, European Institute of Oncology IRCCS, Milan, Italy
[5]Medical Oncology Unit, Ospedali Galliera, 16128 Genova, Italy
[6]Division of Cancer Prevention and Genetics, IEO, European Institute of Oncology IRCCS, Milan, Italy
[7]Experimental Pharmacology Unit, Laboratori di Mercogliano, Istituto Nazionale Tumori, IRCCS-Fondazione G. Pascale, Napoli, Italy
[8]Department of Oncology and Hemato-Oncology, Università Degli Studi di Milano, Milan, Italy
[9]Laboratory of Protein Phosphorylation and Proteomics, Department of Cellular and Molecular Medicine, KU Leuven, Leuven, Belgium
[10]Laboratory of MacroMolecular Cancer Therapeutics (MMCT), Center of Pharmaceutical Sciences, Department of Pharmaceutical Chemistry, University of Vienna, Vienna, Austria
[11]Department of Microbiology, Immunobiology and Genetics, Center for Molecular Biology of the University of Vienna, Max F. Perutz Laboratories, Vienna Biocenter (VBC), 1030 Vienna, Austria
[12]Vienna Metabolomics Center (VIME), University of Vienna, Althanstrasse 14, 1090 Vienna, Austria
[13]Department of Biosciences, University of Milan, 20100 Milan, Italy
[14]Present address: Center of Pharmaceutical Sciences, Department of Pharmaceutical Chemistry, University of Vienna, Vienna, Austria
[15]Lead Contact
*Correspondence: mohamed.elgendy@univie.ac.at (M.E.), saverio.minucci@ieo.it (S.M.)
https://doi.org/10.1016/j.ccell.2019.03.007

## SUMMARY

**Tumor cells may adapt to metabolic challenges by alternating between glycolysis and oxidative phosphorylation (OXPHOS). To target this metabolic plasticity, we combined intermittent fasting, a clinically feasible approach to reduce glucose availability, with the OXPHOS inhibitor metformin. In mice exposed to 24-h feeding/fasting cycles, metformin impaired tumor growth only when administered during fasting-induced hypoglycemia. Synergistic anti-neoplastic effects of the metformin/hypoglycemia combination were mediated by glycogen synthase kinase 3β (GSK3β) activation downstream of PP2A, leading to a decline in the pro-survival protein MCL-1, and cell death. Mechanistically, specific activation of the PP2A-GSK3β axis was the sum of metformin-induced inhibition of CIP2A, a PP2A suppressor, and of upregulation of the PP2A regulatory subunit B56δ by low glucose, leading to an active PP2A-B56δ complex with high affinity toward GSK3β.**

## INTRODUCTION

Therapeutic strategies aimed to tackle metabolic alterations in tumors are gaining greater attention (DeBerardinis and Chandel, 2016; Vander Heiden, 2011). Dietary limitation through caloric restriction (CR) or intermittent fasting (IF) is an emerging approach to target tumor metabolism that has been shown to protect against tumorigenesis and to enhance the response to

### Significance

Targeting tumor metabolism has been considered as an attractive strategy against cancer since the findings of Otto Warburg. This task is, however, complicated by the metabolic plasticity of several tumor cells that can shuffle between glycolysis and mitochondrial OXPHOS, thus escaping the inhibition of either metabolic pathway individually. We present here an effective and safe metabolic strategy to tackle tumors by combining fasting-induced hypoglycemia with metformin, an OXPHOS inhibitor that is used clinically to treat type II diabetes. We dissected the molecular mechanisms of the synergistic effect of the combination and exploited the gained mechanistic insight to tailor pharmacological approaches ready for immediate clinical testing, being based on the repurposing of marketed drugs.

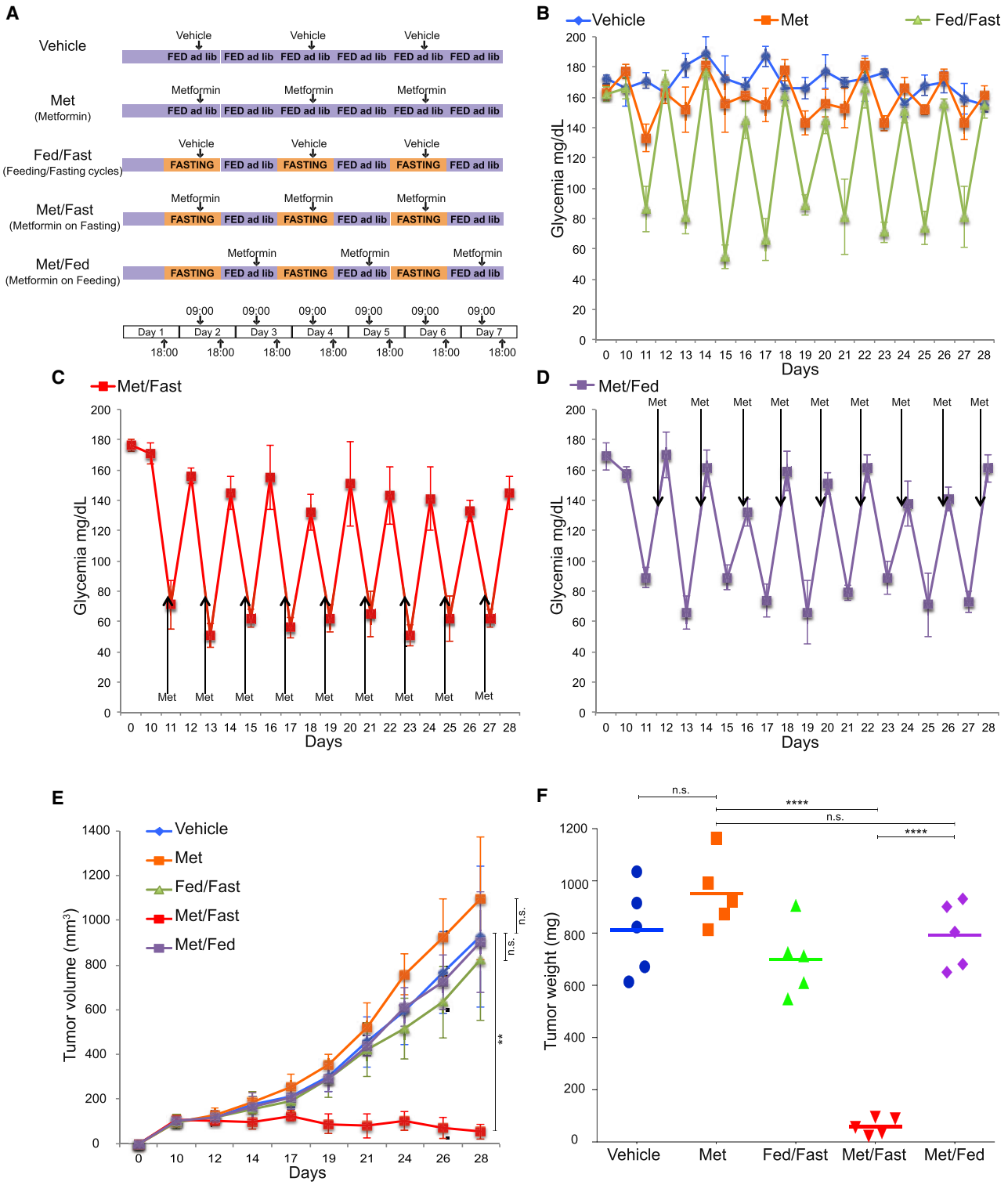


**Figure 1. Intermittent Fasting Sensitizes Tumor-Bearing Mice to Metformin Administered during Hypoglycemic Periods**

(A) Schematic representation of the experimental design showing the feeding protocols and timing of metformin administration in different experimental groups. (B–D) The levels of blood glucose were measured at the end of every feeding/fasting cycle in the experimental groups Vehicle, Met, Fed/Fast (A), Met/Fast (B), and Met/Fed (C). Arrows in (C and D) indicate timing of metformin administration.

*(legend continued on next page)*

chemotherapy (Lee et al., 2012; Longo and Mattson, 2014). CR has been reported to limit tumor growth (Qiu et al., 2010), but its clinical use is complicated by factors such as weight loss, fatigue, nausea, delayed wound healing, and impaired immunity (Lee and Longo, 2011). IF, using a limited time of a severely restricted diet has been shown to protect mice and cancer patients from the toxic effects of chemotherapeutic agents without causing chronic weight loss, making it a possibly safer approach (Raffaghello et al., 2008; Safdie et al., 2009).

Tumor metabolism can also be targeted pharmacologically. Metformin, the most widely used drug for treating type 2 diabetes (T2D), exhibits anti-cancer activities that are supposedly due to its activity on tumor metabolism. Direct effects of metformin on cancer cells have been proposed to involve the activation of the AMP-activated protein kinase (AMPK) (Zhou et al., 2001). However, accumulating reports have described the AMPK-independent anti-proliferative effects of metformin. Metformin has been shown to inhibit mammalian target of rapamycin complex 1 signaling (Kalender et al., 2010) and to decrease phosphorylation of multiple receptor tyrosine kinases, as well as levels of GTP-bound Ras in lung (Quinn et al., 2013), independently of AMPK. Given the favorable safety profile of metformin, several clinical trials are now exploring its potential as an adjuvant cancer therapeutic used in combination with other treatments. Metformin, however, accelerates the growth of BRAF-mutant melanoma cells in preclinical models (Martin et al., 2012). A dual effect of metformin has also been shown in initial clinical studies in breast cancer (Bonanni et al., 2012; DeCensi et al., 2014). Optimization of the clinical use of metformin in cancer would therefore benefit from a better understanding of how it exerts its anti-neoplastic effects.

A shift toward increased glycolysis is a signature of many tumors. Our observations along with emerging reports (DeBerardinis and Chandel, 2016; Havas et al., 2017; Obre and Rossignol, 2015; Pusapati et al., 2016), however, suggest that, in many cases, tumor cells can alternate between dependency on glycolysis or oxidative phosphorylation (OXPHOS) to adapt to metabolic challenges. Targeting one specific metabolic pathway could thus be ineffective. In the present study, we examined the effect of targeting tumor metabolism by a combination of inhibitions of glycolysis and OXPHOS.

## RESULTS

### Hypoglycemia-Metformin Combination Effectively Restrains Tumor Growth

Metformin exerts only weak anti-proliferative effects on an array of cancer cell lines and patient-derived melanoma cells when cells are kept in nutrient-rich conditions (Figure S1A) (Dykens et al., 2008). Treatment of HCT116 cells with metformin was associated with a dose- and time-dependent increase in glucose consumption and lactate production, indicating a switch toward increased glycolysis (Figures S1B–S1E). Conversely, culturing those cells in low glucose conditions induced a rapid increase in oxygen consumption (Figures S1F and S1G), suggesting a shift toward increased OXPHOS. These results suggest that cancer cells may be able to shuffle between OXPHOS and glycolysis to circumvent the inhibition of either process. These findings confirm previous studies that analyzed inhibition of either glycolysis or OXPHOS, and observed an increase in the activity of the other pathway (Hao et al., 2010; Jose et al., 2011; Birsoy et al., 2014; Dykens et al., 2008).

To devise an effective *in vivo* metabolic approach to target tumors, we aimed to simultaneously target alternative metabolic pathways. We examined the effect of a combination of fasting-induced hypoglycemia and metformin in mice bearing xenografts derived from HCT116 cells or from melanoma from two patients (patient-derived xenografts). These mice were distributed into five groups: two groups were kept on *ad libitum* feeding, while three other groups were subjected to 24-h cycles of feeding-fasting, which was achieved by complete withdrawal of food while allowing free access to water (Figure 1A). To test the effect of metformin alone in the absence of IF on tumor growth, one of the two groups on *ad libitum* feeding received vehicle (Vehicle group), while the other received metformin (Met group). To examine the effect of intermittent cycles of fasting on the anti-neoplastic effects of metformin, vehicle or metformin was administered in the three other groups kept on feeding/fasting cycles. The Fed/Fast group received vehicle every 48 h to assess the effect of feeding/fasting cycles alone. The last two groups received metformin every 48 h administered either while the mice were fasted (Met/Fast group) or fed (Met/Fed group). In those three groups exposed to feeding-fasting cycles, all mice were fasted at the same time for 24 h (6 p.m. to 6 p.m of the following day) and vehicle or metformin was administered (9 a.m. of the next day) (Figure 1A). Metformin was thus administered following a period of 15 h of either fasting (Met/Fast) or feeding (Met/Fed) and was allowed to act for the subsequent 9 h before the fasting or feeding cycle was terminated. Metformin has a half-life of around 2.7 h in mice (Um et al., 2007). As expected, fasting cycles resulted in a strong drop in blood glucose and a reduction (1–2 g) in body weight, both of which returned to almost normal levels during the following cycle of feeding (Figures 1B and S1H). Administration of metformin reduced blood glucose levels only slightly (Figure 1B), which is consistent with the observation that metformin can dramatically lower the high glucose levels in T2D patients but has relatively modest effects on subjects with normal glucose levels (Bonanni et al., 2012; Pollak, 2012). Metformin was administered during the hypoglycemia periods in Met/Fast group (Figure 1C) or near the normoglycemic periods in Met/Fed group (Figure 1D). This design allowed us to assess not only the gross effect of IF on the anti-neoplastic activities of metformin but also the effect of the timing of metformin administration during the fasting-feeding cycles. Fasting resulted in a comparable decrease in intra-tumor glucose levels in the three

(E) *In vivo* growth of tumors as measured by tumor volume in mice inoculated with HCT116 cells and treated as shown in (A). Metformin was administered at 200 mg/kg (n = 5 per group).

(F) Weight of tumors isolated from mice in different groups. Horizontal bars indicate median tumor weight. Student's t test was used for statistical analysis (n.s., non-significant). $^{n.s.}p > 0.05$, $^{**}p \leq 0.01$, $^{****}p \leq 0.0001$. Error bars in all the panels of this figure indicate SEM.

See also Figure S1.

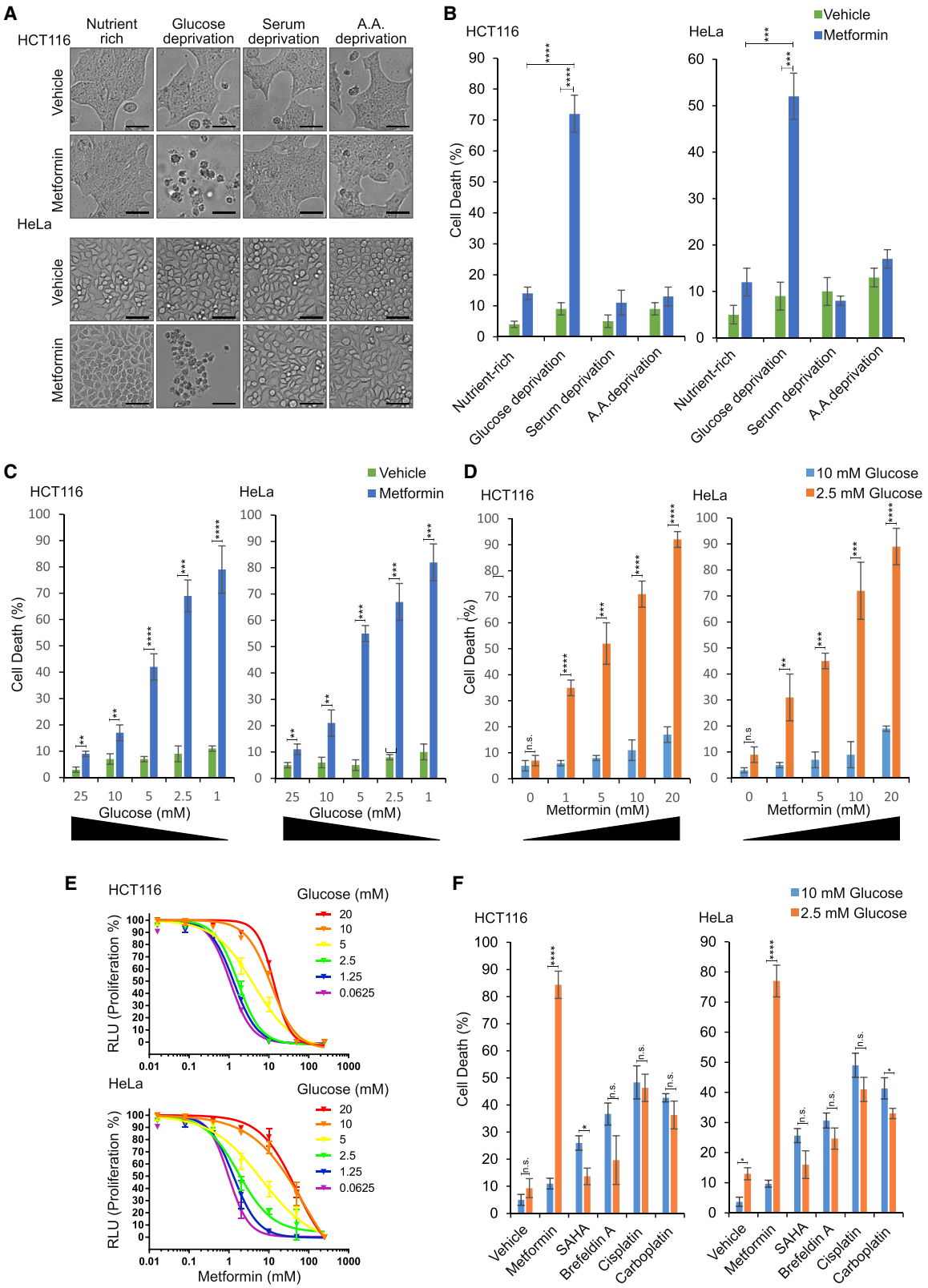


*(legend on next page)*

groups exposed to fasting/feeding cycles (Figure S1I). Metformin alone did not exert any significant tumor-restraining effect. Strikingly, tumor growth was dramatically impaired in the group receiving metformin while fasting (Met/Fast) as compared with all other groups (Figures 1E and 1F), indicating that the anti-proliferative effects of metformin were highly and specifically enhanced when it was administered during the hypoglycemia periods of a schedule of IF.

### Activation of GSK3β Mediates the Synergistic Cytotoxicity of Low Glucose/Metformin Combination

Fasting reduces the blood levels of glucose but it also results in a decrease in circulating growth factors and nutrients (Lee and Longo, 2011). To examine which of these factors contribute to the observed sensitization of tumor cells to metformin, HCT116 and HeLa cells were cultured under glucose, serum, or amino acid (A.A.) deprivation conditions in the presence or absence of metformin. Cells cultured under nutrient-rich conditions with or without metformin served as control. In agreement with recent reports (Birsoy et al., 2014; Zhuang et al., 2014), deprivation of glucose, but not serum or A.A., sensitized cells to metformin (Figures 2A, 2B, S2A, and S2B). The Chou-Talalay combination index was <1, indicating synergy among treatments. Cells sequentially treated with metformin and low glucose did not show the same magnitude of cell death observed in cells treated simultaneously with the combination (Figure S2C). The synergistic effect between metformin treatment and glucose deprivation depended on both metformin concentration and glucose levels (Figures 2C–2E, S2D, and S2E), and was observed in several cancer cell lines as well as patient-derived melanoma cells (Figure S2F), suggesting that it is a general phenomenon. This effect also seemed to be specific to metformin as glucose deprivation did not sensitize cells to other cytotoxic agents (Figure 2F).

The activation of AMPK is the most widely accepted mechanism to explain the anti-cancer effects of metformin. Immunoblotting analysis showed that AMPK phosphorylation was slightly enhanced by the metformin/low glucose combination (Figure S3A), which correlated with an increase in AMP/ATP ratio in those cells (Figure S3B), in HCT116 cells but it was almost completely abolished by the combination in HeLa cells (Figure S3A). The same synergistic cytotoxicity but different AMPK phosphorylation in HCT116 and HeLa cells treated with the metformin/low glucose combination suggested that AMPK may not be mediating the cytotoxic phenotype. Indeed, depletion of AMPK in HCT116 (Figures S3C–S3E) or expression of a constitutively active form of AMPK in HeLa cells (Figures S3F–S3H) failed to modulate the synergistic cytotoxicity observed in both cell lines to a significant extent. In both cases, phosphorylation of acetyl-CoA carboxylase, a known downstream target of AMPK, was used to monitor AMPK activity (Figures S3C and S3F). Taken together, these results suggest that the observed synergistic cytotoxicity of the metformin/low glucose combination is AMPK independent.

To identify the signaling pathway(s) mediating the observed synergistic cytotoxicity between metformin and low glucose, we screened a battery of kinase inhibitors. The results showed that cells treated with inhibitors of glycogen synthase kinase 3β (GSK3β) were resistant to the low glucose/metformin combination (Figure 3A). GSK3β is a Ser/Thr kinase that is known to play crucial roles in the regulation of protein synthesis, cell proliferation, differentiation, motility, and apoptosis (Cohen and Frame, 2001). Phosphorylation of GSK3β at serine 9 inhibits its activity, and it is thus commonly used as a marker for the inactive GSK3β. Immunoblotting analysis revealed an almost completely abolished GSK3β phosphorylation (and thus hyperactivation) in cells on low glucose-metformin treatment (Figures 3B and S3I). Notably, GSK3β dephosphorylation by the low glucose/metformin combination was consistently observed in all cells, in contrast to the differential effect on AMPK and extracellular signal-regulated kinase phosphorylation (Figure 3B). Interestingly, GSK3β was dephosphorylated only by the combination, while either metformin or low glucose alone—if anything—slightly increased the level of GSK3β phosphorylation (Figures 3B and S3I). GSK3β de-phosphorylation by the combination depended on the concentration of metformin and negatively correlated with that of glucose (Figures 3C–3D). Furthermore, the combination of metformin and 2-deoxyglucose, a glucose analog that inhibits glycolysis, resulted in a similar dramatic reduction in GSK3β phosphorylation (Figure S3J), which correlated with the synergistic cytotoxicity of this combination even in cells cultured in glucose-rich conditions (Figure S3K). Finally, consistent with the data obtained using pharmacological inhibitors, GSK3β-depleted cells treated with low glucose plus metformin proliferated almost normally and did not show cell death observed in control cells (Figures 3E–3G and S3L), further confirming an essential role for GSK3β in mediating the synergistic cytotoxicity of low glucose and metformin combination.

**Figure 2. Glucose Starvation Sensitizes Cancer Cells to Metformin**

(A) Images of HCT116 and HeLa cells cultured for 24 h in nutrient-rich (10% FBS and 10 mM glucose), glucose-deprived (10% FBS and 2.5 mM glucose), serum-deprived (0.1% serum and 10 mM glucose), or A.A.-deprived (10% FBS and 10 mM glucose but no glutamine, no methionine, and no cysteine) DMEM. Media were replenished every 6 h. Scale bars, 100 μm.

(B) Quantification of cell death of HCT116 and HeLa cells cultured as in (A).

(C and D) Percentage of cell death of HCT116 and HeLa cells cultured for 24 h in DMEM containing the indicated concentrations of glucose in the absence or presence of 5 mM (C) or the indicated concentrations (D) of metformin.

(E) Proliferation assessed by CellTiter-Glo assay of HCT116 and HeLa cells cultured in DMEM containing the indicated concentration of glucose and treated with increasing concentrations of metformin for 24 h.

(F) Percentage of cell death of HCT116 and HeLa cells cultured for 24 h in DMEM containing either 10 or 2.5 mM glucose in combination with metformin (5 mM), SAHA (2.5 μM), brefeldin A (10 μM), cisplatin (100 μM), or carboplatin (400 μM). Media were replenished every 6 h. Results are representative of three biologically independent experiments.

Error bars in all the panels of this figure indicate SD. Student's t test was used for statistical analysis (n.s., non-significant). $^{n.s.}p > 0.05$, $^{*}p \leq 0.05$, $^{**}p \leq 0.01$, $^{***}p \leq 0.001$, $^{****}p \leq 0.0001$. See also Figure S2.

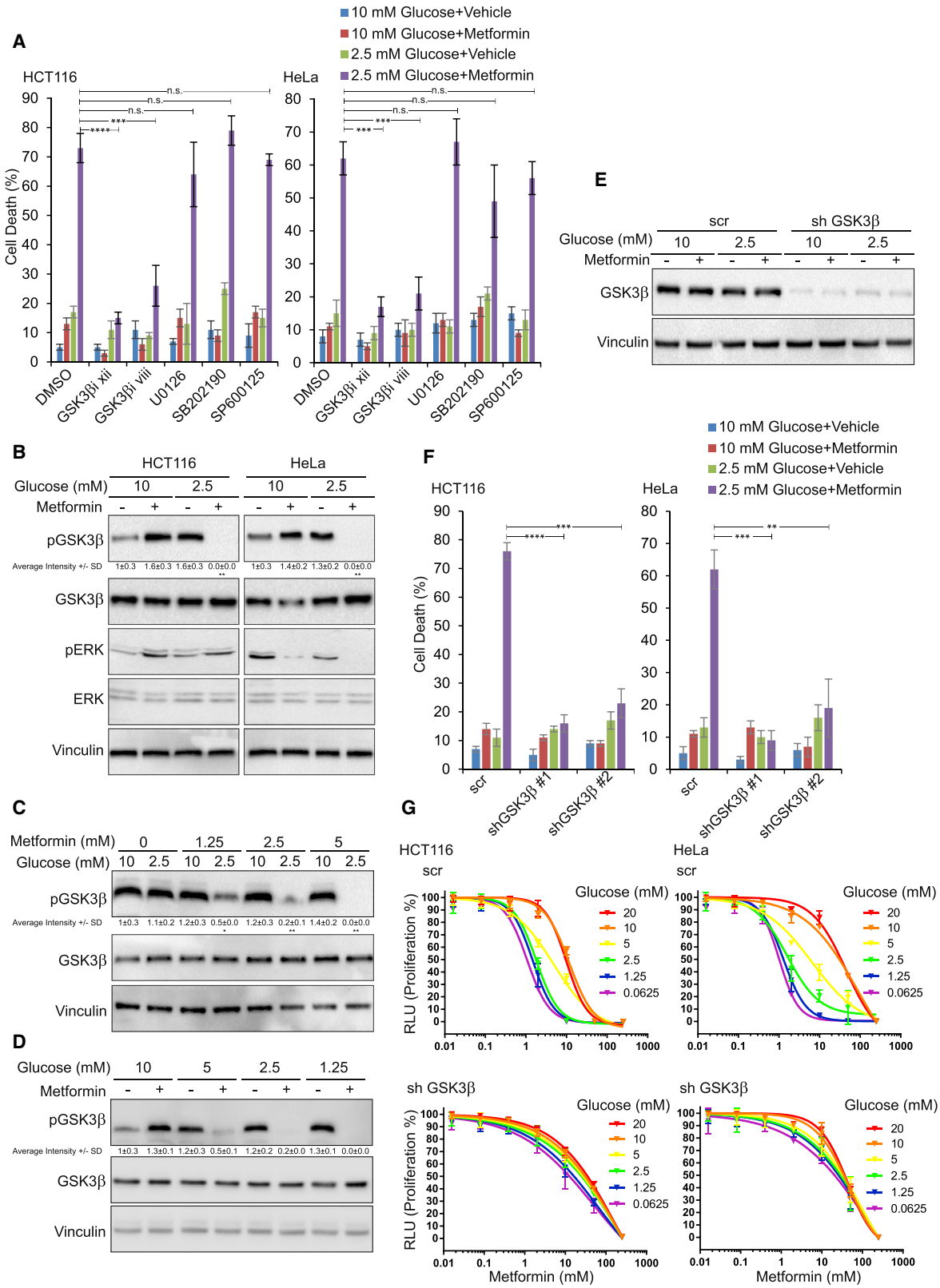


*(legend on next page)*

### A GSK3β-Dependent Decline in MCL-1 Levels Mediates the Synergistic Cytotoxicity of the Low Glucose/Metformin Combination

Phosphorylation by GSK3β and subsequently enhanced proteasomal degradation of MCL-1, a pro-survival member of the BCL-2 family of proteins, mediates cell death triggered by GSK3β activation (Maurer et al., 2006; Wang et al., 2012).

Immunoblotting analysis showed that metformin treatment of cells cultured in low glucose, but not on serum or A.A. starvation, resulted in a marked reduction in MCL-1, but not other BCL-2 family members or protein levels, confirming the specificity of MCL-1 modulation (Figures 4A, 4B, and S4A). The decline in MCL-1 levels correlated with GSK3β activation (Figures 4A and 4B) and depended on both metformin and glucose concentrations (Figures 4C and 4D). The immunoblotting analysis showed that metformin/low glucose combination did not result in reduction in MCL-1 levels in cells depleted of GSK3β, unlike control cells (Figure 4E), indicating that the decline in MCL-1 levels is indeed mediated by GSK3β. Consistently, cells treated with a pharmacological inhibitor of GSK3β did not show the decline in MCL-1 levels observed in control cells on treatment with metformin and low glucose combination (Figure S4B).

Finally, we tested whether the GSK3β-mediated decline in MCL-1 levels contributes to the synergistic cytotoxicity between metformin and low glucose. We found that cells overexpressing MCL-1 were more resistant to cell death than control cells or cells overexpressing BCL-2 or BCL-xL on treatment with metformin in low glucose conditions (Figures 4F, 4G, and S4C). The rescue of cell death reproducibly correlated with the level of MCL-1 overexpression (Figures S4C–S4H). MCL-1 is thus a main mediator of the cytotoxicity of the combination downstream of GSK3β, although we cannot rule out the potential contribution of other GSK3β targets with established functions in coordinating cell fate and metabolism such as c-myc (Stine et al., 2015). Indeed, metformin alone and, more significantly, in combination with low glucose, also modulates the levels of c-myc (Figure S4I) (Akinyeke et al., 2013). Other pathways that may be modulated by the metformin/low glucose combination remain to be further investigated.

Akt has been established as a major kinase that phosphorylates GSK3β (Cohen and Frame, 2001). However, the dramatic decline in phospho-GSK3β by the low glucose-metformin combination did not correlate with marked changes in the phosphorylation of Akt or GSK3α (Figure S4I). We therefore focused on the potential role of phosphatases that may mediate GSK3β dephosphorylation.

### PP2A Mediates the Synergistic Cytotoxicity of Low Glucose/Metformin Combination

Protein phosphatase 2A (PP2A) is a major serine-threonine phosphatase in mammalian cells that acts as a tumor suppressor. Recently, we have shown that PP2A coordinates a link between metabolism and DNA damage response in yeast (Ferrari et al., 2017). PP2A has been shown to regulate GSK3β activity by removing phosphorylation at serine 9 and other regulatory residues (Bennecib et al., 2000; Mitra et al., 2012). We examined whether PP2A contributed to the synergistic cytotoxicity of metformin and low glucose and found that PP2A-depleted cells did not show a decline in GSK3β phosphorylation or MCL-1 levels in the metformin/low glucose combination (Figure 5A) and were more resistant to cell death compared with control cells (Figures 5B, 5C, and S5A). These results implicated PP2A as a key regulator of the cytotoxicity of the combination of low glucose with metformin.

Next, we investigated a pharmacological approach that could be more clinically feasible to mimic the effect of low glucose treatment. Our data showed that a combination of metformin with perphenazine (PPZ), a US Food and Drug Administration-approved anti-psychotic drug that has been shown to modulate PP2A (Gutierrez et al., 2014), diminished the levels of phosphorylated GSK3β and total MCL-1 (Figure S5B). Consistently, PPZ sensitized cells to metformin, but not other cytotoxic agents (Figures S5C–S5F). The synergism of the metformin-PPZ combination was mediated by PP2A, as cells depleted of PP2A were resistant to the combination (Figure S5G) and did not show the reduction of phosphorylated GSK3β and MCL-1 levels observed in control cells treated with the combination (Figure S5H). Consistent with the *in vitro* results, PPZ also synergized with metformin in impairing the growth of tumor xenografts *in vivo* (Figures S5I and S5J). Thioridazine, another PP2A activator (Chien et al., 2015) that we found to diminish phosphorylated GSK3β and MCL-1 levels when combined with metformin (Figure S5B), exerted synergistic cytotoxic effects with metformin similar to PPZ (Figure S5K).

**Figure 3. Synergistic Cytotoxicity of Low Glucose and Metformin Is Mediated by GSK3β**

(A) Percentage of cell death of HCT116 and HeLa cells treated with either the GSK3β inhibitor xii (20 μM), GSK3 β inhibitor viii (25 μM), ERK inhibitor U0126 (20 μM), p38 inhibitor SB202190 (20 μM), or JNK inhibitor SP600125 (20 μM), and cultured for 24 h in DMEM (replenished every 6 h) containing either 10 or 2.5 mM glucose in the absence or presence of metformin (5 mM). Treatment with the inhibitors started 1 h before metformin treatment.

(B) Immunoblotting analysis of lysates derived from HCT116 and HeLa cells cultured for 24 h in DMEM (replenished every 6 h) containing either 10 or 2.5 mM glucose in the absence or presence of metformin (5 mM).

(C and D) Immunoblotting analysis of lysates derived from HCT116 cells cultured for 24 h in DMEM (replenished every 6 h) containing the indicated concentrations of glucose in the absence or presence of the indicated concentrations (C) or 5 mM (D) of metformin.

(E) Immunoblotting analysis of lysates derived from HCT116 cells stably expressing either scrambled small hairpin RNA (shRNA) or shRNA against GSK3β and treated as in (B).

(F) Percentage of cell death of control or GSK3β-depleted HCT116 and HeLa cells treated as in (B).

(G) Proliferation assessed by CellTiter-Glo assay of control or GSK3β-depleted HCT116 and HeLa cells cultured in DMEM containing the indicated concentration of glucose and treated with increasing concentrations of metformin for 24 h. Results are representative of three biologically independent experiments.

Error bars in all the panels of this figure indicate SD. Average intensities of the bands from three biologically independent repeats normalized to loading control and expressed as fold change of the first band ± SD are presented under each lane. Student's t test was used for statistical analysis (n.s., non-significant). $^{n.s.}p > 0.05$, $^{*}p \leq 0.05$, $^{**}p \leq 0.01$, $^{***}p \leq 0.001$, $^{****}p \leq 0.0001$. See also Figure S3.

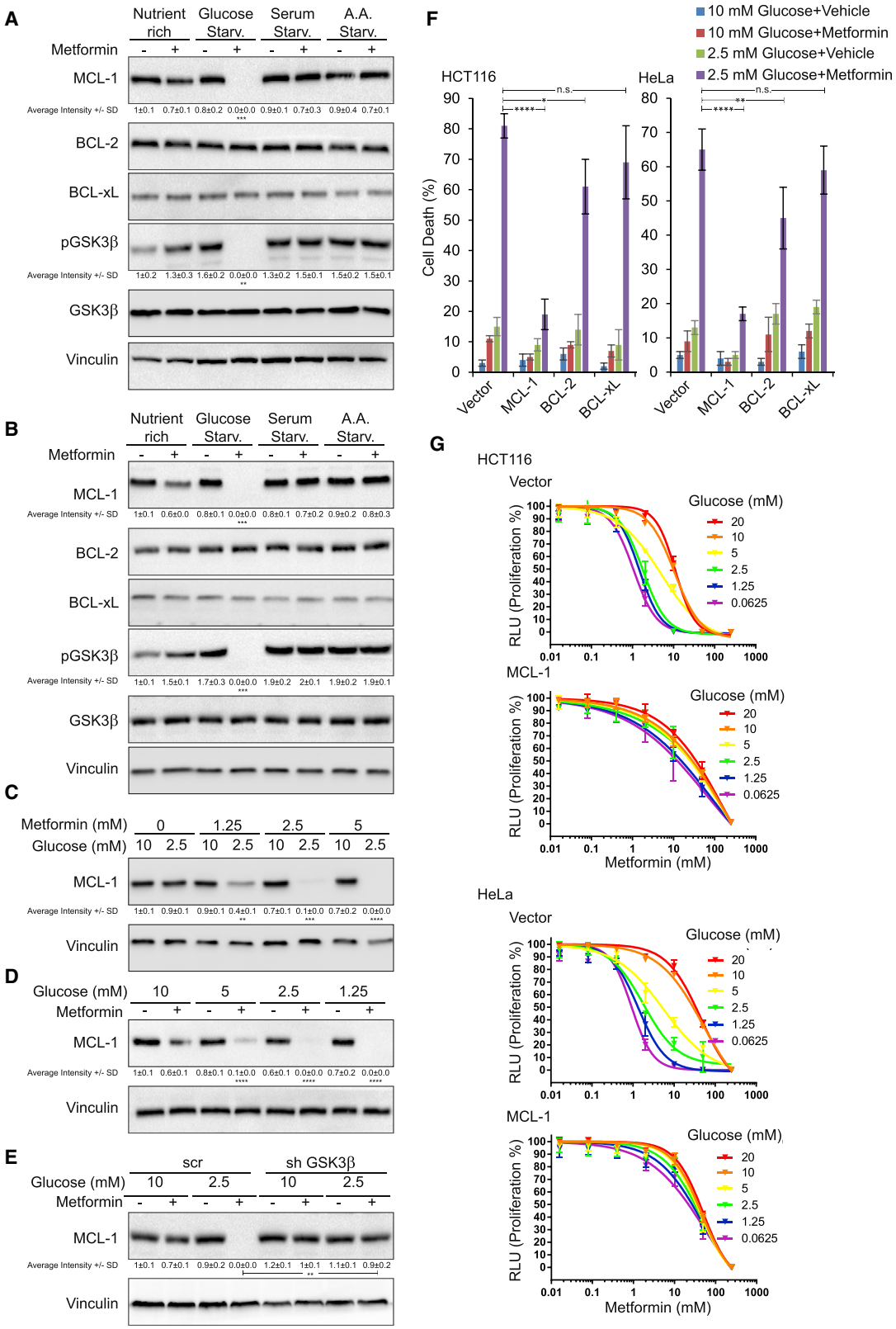


*(legend on next page)*

### Upregulation of the PP2A Regulatory Subunit B56δ and Downregulation of CIP2A Mediate the Effects of the Low Glucose/Metformin Combination

PP2A is a trimeric protein complex consisting of a catalytic subunit (PP2Ac or C), a scaffold subunit (PR65 or A), and one of several regulatory B subunits. Such variability in PP2A composition results in heterogeneity in the composition of active PP2A holoenzymes, each with unique substrates and functions (Janssens et al., 2005). The B subunit incorporated in a holoenzyme modulates its substrate specificity, subcellular targeting, and phosphatase activity. The activity of PP2A is also regulated by inhibitors: cancerous inhibitor of protein phosphatase 2A (CIP2A) is an endogenous PP2A inhibitor that is overexpressed in several types of cancer and contributes to malignant transformation through inhibition of PP2A (Junttila et al., 2007).

Immunoblotting analysis showed that metformin treatment reduced the CIP2A level, low glucose treatment increased the regulatory PP2A subunit B56δ level, and the combination of metformin with low glucose simultaneously reduced CIP2A and increased B56δ levels (Figures 6A and S6A). These modulations are initiated shortly after treatment with the metformin/low glucose combination (Figure 6B), further implicating PP2A as an early sensor of metabolic stress and a coordinator of subsequent responses in this context. Modulation of CIP2A and B56δ levels was also dependent on both metformin concentration and glucose levels (Figures S6B and S6C), and, while low glucose induced the transcription of *PPP2R5D*, the gene encoding B56δ (Figures S6D), metformin mainly promoted CIP2A proteasomal degradation as it failed to diminish CIP2A levels in the presence of proteasome inhibitors (Figures S6E–S6G).

GSK3β is an established substrate of the PP2A holoenzyme containing B56δ (Lambrecht et al., 2018; Haesen et al., 2016). These results therefore suggested that PP2A is activated by metformin through inhibition of its suppressor CIP2A; because low glucose induces B56δ expression, the metformin/low glucose combination favors the formation of an active PP2A complex containing the B56δ subunit, which then targets GSK3β for dephosphorylation, ultimately leading to MCL-1 downregulation and cell death.

To test this hypothesis, we overexpressed CIP2A and found that overexpression of CIP2A halted the decline in phosphorylated GSK3β and MCL-1 levels and the induction of cell death observed in cells on treatment with the combination of metformin with low glucose (Figures 6C–6E and S6H). Furthermore, depletion of CIP2A was sufficient to recapitulate the effects of metformin as the combination of CIP2A depletion with low glucose triggered a decline in phosphorylated GSK3β and MCL-1 levels and evoked cell death comparable with that observed with the metformin/low glucose treatment (Figures 6F and 6G). These results thus suggest that metformin-induced downregulation of CIP2A mediates PP2A activation and can be attributed for—largely, if not all—sensitization of cells to low glucose conditions.

### Formation of an Active PP2A Holoenzyme Containing B56δ Mediates Cytotoxicity of the Combination of Low Glucose with Metformin

Next, we aimed to examine the contribution of low glucose-induced B56δ upregulation to the synergistic cytotoxicity. The combination of low glucose and metformin did not result in reduced levels of phosphorylated GSK3β and MCL-1 in B56δ-depleted cells, unlike control cells or cells depleted of another B regulatory subunit B55α (Figure 7A). Consistently, B56δ-depleted cells were more resistant to the combination of low glucose with metformin (Figures 7B, 7C, and S7A). We then examined the composition of the PP2A holoenzyme complex under different conditions. Consistent with our hypothesis, using immunoprecipitation of the PP2A Aα subunit, we observed an enhanced recruitment of B56δ and GSK3β to the PP2A holoenzyme in cells treated with the combination of low glucose with metformin (Figure 7D). Furthermore, reconstitution with the wild-type PP2A Aα, but not the PP2A Aα S256F mutant, which altered activity of the PP2A-B56δ complex (Haesen et al., 2016), restored GSK3β dephosphorylation and MCL-1 downregulation in PP2A Aα-ablated cells treated with the low glucose/metformin combination (Figure 7E). Overexpression of B56δ and subsequent enrichment of a B56δ-containing PP2A holoenzyme (Figure S7B) synergized with metformin, but not SAHA or brefeldin A, to induce GSK3β dephosphorylation, MCL-1 downregulation (Figure 7F), and cell death (Figures 7G, S7C, and S7D). B56δ overexpression thus recapitulated the effects of low glucose in the combination with metformin. Consistently, PPZ and thioridazine—which are synergistic in combination with metformin—enriched for the PP2A holoenzyme containing the B56δ subunit and increased recruitment of GSK3β (Figures S5B and S7E).

**Figure 4. GSK3β-Depleted MCL-1 Degradation Mediates Synergistic Cytotoxicity of Low Glucose and Metformin**

(A and B) Immunoblotting analysis of lysates derived from HCT116 (A) and HeLa (B) cells cultured for 24 h in nutrient-rich (10% FBS and 10 mM glucose), glucose-deprived (DMEM containing 10% FBS and 2.5 mM glucose), serum-deprived (0.1% serum and 10 mM glucose), or A.A.-deprived (10% FBS and 2.5 mM glucose but no glutamine, no methionine and no cysteine) DMEM. Media were replenished every 6 h.

(C and D) Immunoblotting analysis of lysates derived from HCT116 cells cultured for 24 h in DMEM (replenished every 6 h) containing the indicated concentrations of glucose in the absence or presence of the indicated concentrations (C) or 5 mM (D) of metformin.

(E) Immunoblotting analysis of lysates derived from HCT116 cells expressing either scrambled shRNA or shRNA against GSK3β and cultured for 24 h in DMEM (replenished every 6 h) containing either 10 or 2.5 mM glucose in the absence or presence of metformin (5 mM).

(F) Percentage of cell death of HCT116 and HeLa cells expressing the indicated constructs and cultured as in (D).

(G) Cellular proliferation measured by CellTiter-Glo of control or MCL-1-overexpressing HCT116 and HeLa cells cultured in DMEM containing the indicated concentration of glucose and treated with increasing concentrations of metformin for 24 h. Results are representative of three biologically independent experiments.

Error bars in all the panels of this figure indicate SD. Average intensities of the bands from three biologically independent repeats normalized to loading control and expressed as fold change of the first band ± SD are presented under each lane. Student's t test was used for statistical analysis (n.s., non-significant). $^{n.s.}p > 0.05$, $^{*}p \leq 0.05$, $^{**}p \leq 0.01$, $^{***}p \leq 0.001$, $^{****}p \leq 0.0001$. See also Figure S4.

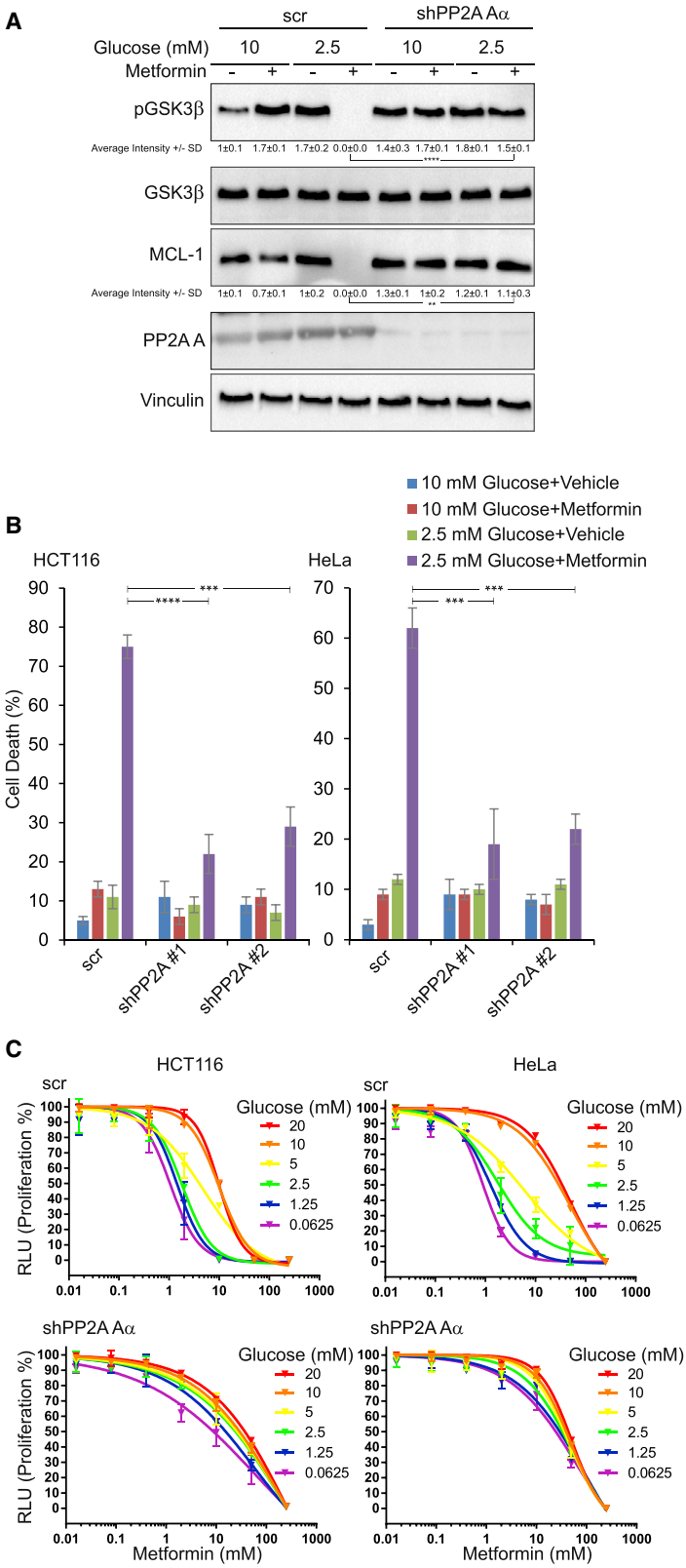


**Figure 5. PP2A-Regulated GSK3β Dephosphorylation Mediates Synergistic Cytotoxicity of Low Glucose and Metformin**

(A) Immunoblotting analysis of lysates derived from HCT116 cells expressing either scrambled shRNA or shRNA against PP2A and cultured for 24 h in DMEM (replenished every 6 h) containing either 10 or 2.5 mM glucose in the absence or presence of metformin (5 mM).

(B) Percentage of cell death of control or PP2A-depleted HCT116 and HeLa cells treated as in (A).

(C) Proliferation assessed by CellTiter-Glo assay of control or PP2A-depleted HCT116 and HeLa cells cultured in DMEM containing the indicated concentration of glucose and treated with increasing concentrations of metformin for 24 h. Results are representative of three biologically independent experiments. Average intensities of the bands from three biologically independent repeats normalized to loading control and expressed as fold change of the first band ± SD are presented under each lane.

Error bars in all the panels of this figure indicate SD. Student's t test was used for statistical analysis. $^{**}p \leq 0.01$, $^{***}p \leq 0.001$, $^{****}p \leq 0.0001$. See also Figure S5.

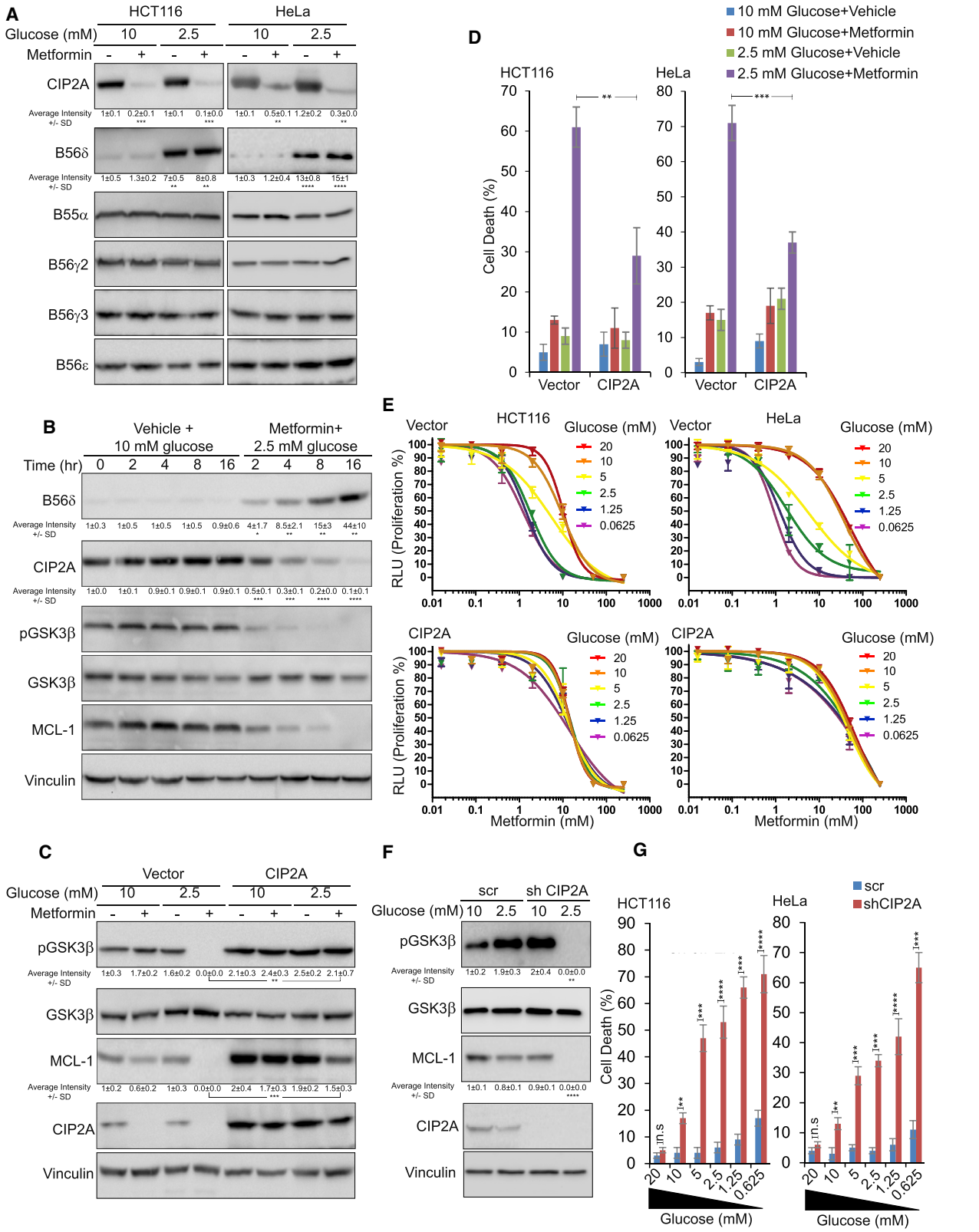


*(legend on next page)*

### Tumors Depleted of GSK3β or Overexpressing MCL-1 and/or CIP2A Are Resistant to Metformin Administered during Fasting

We then examined whether the mechanistic model derived from the *in vitro* studies described above accounts for the tumor-restraining effect of the metformin/hypoglycemia combination *in vivo*. Immunohistochemistry analysis of tumor tissues derived from the *in vivo* experiment in the Figure 1 showed that the levels of MCL-1 and phosphorylated GSK3β in the tissues derived from mice treated with metformin while fasting (Met/Fast group) were markedly lower compared with the other experimental groups (Figures 8A and 8B). Immunoblotting analysis of tumor lysates prepared from Met/Fed against Met/Fast mice showed that administration of metformin to hypoglycemic (fasting) mice resulted in a decrease in MCL-1 and CIP2A levels and GSK3β phosphorylation and, conversely, in an increase in B56δ levels (Figure 8C) and concomitant recruitment of B56δ and GSK3β to the PP2A holoenzyme (Figure S8A), all events which correlated with induction of caspase-dependent cell death (Figure S8B). These results suggest that the metformin/hypoglycemia combination elicited molecular events in tumors similar to those observed *in vitro*. Perturbation of these events by overexpression of MCL-1 or CIP2A, or knockdown of GSK3β or B56δ, enhanced the clonogenicity of HCT116 cells treated with metformin/low glucose combination and subjected to *in vitro* clonogenic assays (Figures S8C and S8D). To test whether perturbation of the identified pathway can similarly affect the tumor-restraining effects of metformin/hypoglycemia *in vivo*, we monitored the growth of GSK3β-depleted or MCL-1-overexpressing tumors in mice kept on 24-h feeding/fasting cycles with half the mice from each group receiving metformin every 48 h during either feeding or fasting cycles as previously explained (see Figure 1A). Unlike control tumors, tumors derived from GSK3β-depleted or MCL-1-overexpressing cells grew similarly in both conditions and metformin/hypoglycemia combination failed to exert a growth inhibitory effect (Figures 8D and 8E). Similarly, tumors ectopically overexpressing CIP2A were resistant to metformin/hypoglycemia combination compared with control tumors, which were sensitive to metformin (but not to cisplatin) administrated during hypoglycemia (Figures S8E and S8F). Finally, tumor cell lines that endogenously express high levels of CIP2A and/or MCL-1 were resistant to metformin/low glucose combination *in vitro* (Figures S8G–S8I), and tumors derived from those cells as well as patient-derived xenografts expressing high levels of CIP2A/MCL-1 were refractory to metformin/hypoglycemia combination *in vivo* in contrast to tumor cells and tumors with low CIP2A and/or MCL-1 levels (Figures S8J and S8K).

Collectively, these results highlight the crucial role of the PP2A-GSK3β-MCL-1 axis in mediating the synergistic anti-proliferative effect of metformin/low glucose *in vitro* and similarly metformin/hypoglycemia *in vivo* and suggest that modulation of this axis can serve as an effective approach to tackle tumor metabolic plasticity (Figure 8F).

## DISCUSSION

In the present study, we exploited IF as a clinically feasible, safe, and effective approach to lower glucose availability and explored the potential synergistic effect of a combination of IF with the OXPHOS inhibitor metformin on tumor growth. Our results suggest that both IF and the timing of metformin administration during the fasting/feeding cycles dictate the sensitivity of tumors to metformin. Although the fasting protocol was well-tolerated in mice, the effect on tumor growth was dramatic combined with metformin treatment (Met/Fast). There was no significant correlation between reduction in intra-tumor glucose levels and tumor weight between the Met/Fast group and either the Fast ($p = 0.895$) or Met/Fed groups ($p = 0.923$), suggesting that the dramatic inhibitory effect of metformin/hypoglycemia combination could not simply be attributed to further reduction of glucose levels in tumors. The fasting cycle resulted in only a transient weight loss, and metformin did not cause additional weight loss or any other signs of toxicity when combined with fasting in the Met/Fast group, which showed the most dramatic reduction in tumor growth. The weight loss observed is relatively modest, especially compared with the weight loss observed in mice treated with established anti-cancer drugs. However, given the differences in fat and body mass between mice and humans, it remains to be investigated whether this protocol could be equally well-tolerated in patients.

*In vitro*, glucose deprivation phenocopied the effect of fasting and dramatically sensitized a panel of tumor cells to metformin. These results are consistent with previous studies reporting the synergism of the metformin/low glucose combination (Birsoy et al., 2014; Zhuang et al., 2014). Birsoy and colleagues showed that cancer cells may cope with the metabolic stress exerted by glucose deprivation by upregulating compensatory OXPHOS,

**Figure 6. Metformin-Induced Downregulation of CIP2A Contributes to Synergistic Cytotoxicity of Low Glucose/Metformin Combination**

(A) Immunoblotting analysis of lysates used in the Figure 3B.

(B) Immunoblotting analysis of lysates derived from HCT116 cells cultured for the indicated time points in DMEM containing either 10 mM glucose and vehicle or 2.5 mM glucose and 5 mM metformin.

(C) Immunoblotting analysis of lysates derived from HCT116 cells expressing either vector or CIP2A constructs and cultured for 24 h in DMEM (replenished every 6 h) containing either 10 or 2.5 mM glucose in the absence or presence of metformin (5 mM).

(D) Percentage of cell death of HCT116, HeLa cells treated as in (C).

(E) Proliferation assessed by CellTiter-Glo assay of control or CIP2A-overexpressing HCT116 and HeLa cells cultured in DMEM containing the indicated concentration of glucose and treated with increasing concentrations of metformin for 24 h.

(F) Immunoblotting analysis of lysates derived from HCT116 cells stably expressing scrambled shRNA or shRNAs against CIP2A and cultured for 24 h in DMEM (replenished every 6 h) containing either 10 or 2.5 mM glucose.

(G) Percentage of cell death of HCT116, HeLa cells treated as in (F). Results are representative of three biologically independent experiments.

Error bars in all the panels of this figure indicate SD. Average intensities of the bands from three biologically independent repeats normalized to loading control and expressed as fold change of the first band ± SD are presented under each lane. Student's t test was used for statistical analysis (n.s., non-significant). $^{n.s.}p > 0.05$, $^{*}p \leq 0.05$, $^{**}p \leq 0.01$, $^{***}p \leq 0.001$, $^{****}p \leq 0.0001$. See also Figure S6.

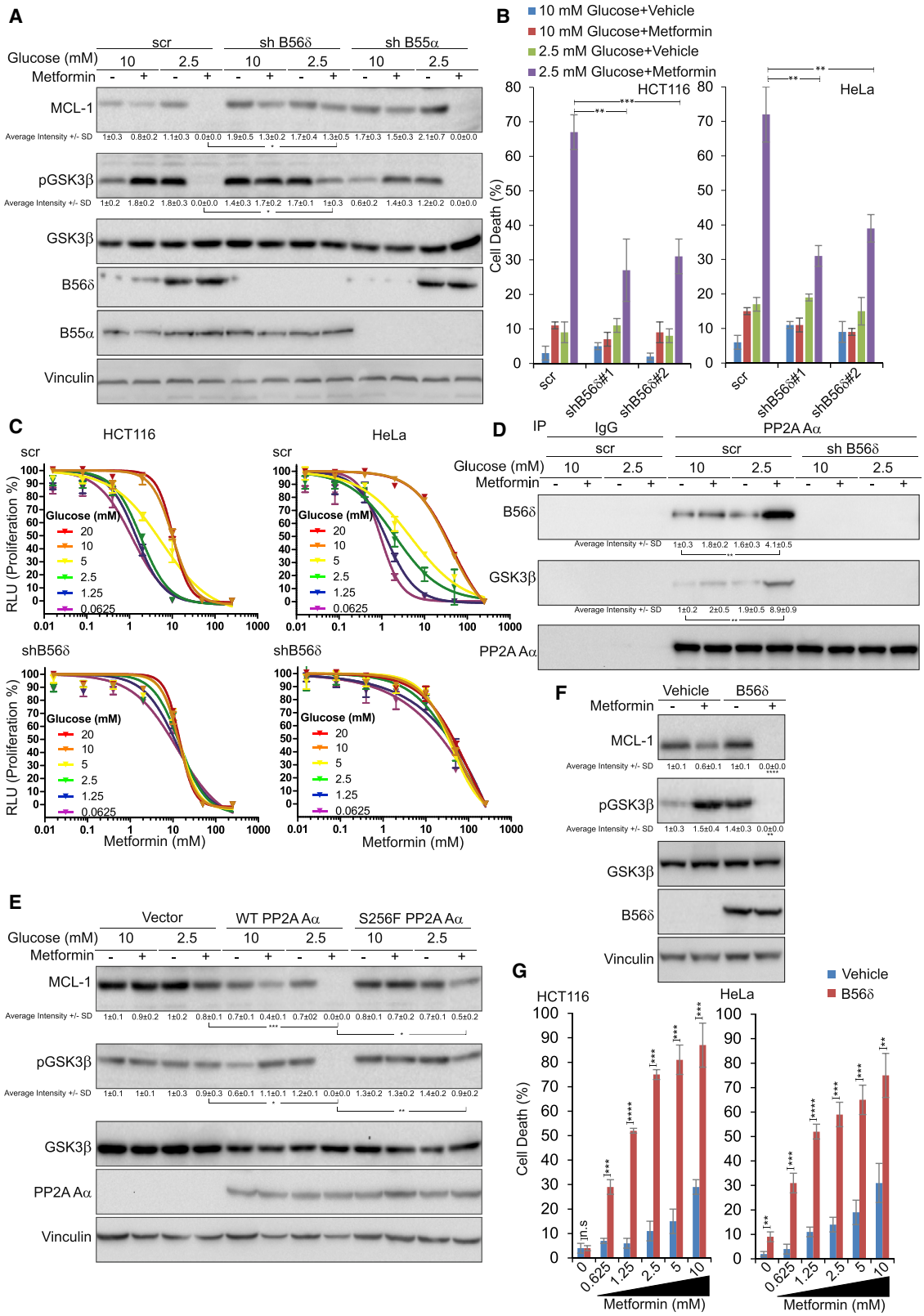


**Figure 7. Low-Glucose-Induced B56δ Upregulation Contributes to Synergistic Cytotoxicity of Low-Glucose/Metformin Combination**

(A) Immunoblotting analysis of lysates derived from HCT116 cells stably expressing scrambled shRNA or shRNAs against either B56δ or B55α and cultured for 24 h in DMEM (replenished every 6 h) containing either 10 or 2.5 mM glucose in the absence or presence of metformin (5 mM).

*(legend continued on next page)*

which renders them sensitive to OXPHOS inhibition by metformin or phenformin. Cancer cells with reduced OXPHOS due to either mutated mitochondrial DNA or impaired glucose utilization were unable to initiate this adaptive response, and were thus particularly sensitive to glucose deprivation to one-tenth of normal levels (Birsoy et al., 2014). While glucose levels in the tumor micro-environment are low, the physiological relevance of such drastic glucose deprivation is unclear.

We report here that cell death in response to the combination of metformin with moderate glucose deprivation is not the consequence of a passive series of events, but is the final outcome of a tightly coordinated signaling process that orchestrated molecular events distinct from the events triggered by either treatment alone. Our molecular analysis initially ruled out a central role for AMPK in mediating the cellular responses trigged by the combination of low glucose with metformin. The unexpected independency of AMPK was intriguing given the well-established role of AMPK in mediating the response to either metformin or low glucose individually, but it is in line with reports showing that AMPK is not required for the action of metformin on cancer cells (Kalender et al., 2010; Quinn et al., 2013).

Further mechanistic investigation showed that cell death in response to the combination is mediated by specific modulation of the PP2A-GSK3β-MCL-1 axis whereas PP2A dephosphorylates and thus activates GSK3β, which in turn acts to diminish MCL-1 levels and ultimately leading to cell death and reduction of tumor growth.

Our findings thus establish a critical role for PP2A as an early-response sensor of the energetic stress triggered in our model by simultaneous inhibition of alternative metabolic pathways by a combination of metformin and low glucose. Interestingly, in line with our findings, it has been shown that simultaneous targeting of multiple metabolic pathways through inhibition of nutrient uptake triggered PP2A activation (Kim et al., 2016).

PP2A has been established as a tumor suppressor, and the inactivation of PP2A has become widely accepted as an important step toward full-blown transformation. Indeed, genetic and/or functional inactivation of different PP2A subunits, and, therefore, loss of its phosphatase activity, have been found in several types of tumors (Janssens et al., 2005; Mumby, 2007). Particularly, the B56δ-containing PP2A complex plays important tumor suppressor roles through its established function in the regulation of GSK3β dephosphorylation (Lambrecht et al., 2018; Haesen et al., 2016) and possibly other substrates.

Activation of PP2A has emerged as a promising therapeutic strategy in cancer, potentially capable of overcoming drug resistance induced in patients by continuous exposure to kinase inhibitors. Orally bioavailable small-molecule activators of PP2A have been shown to inhibit the growth of KRAS-mutant lung cancers in mouse xenografts and transgenic models (Sangodkar et al., 2017). Importantly, PPZ exploited in this study is approved for clinical use as an anti-psychotic: we therefore suggest investigating whether its PP2A-inducing activity could be exploited for repurposing it as an anti-cancer agent (Gutierrez et al., 2014).

In addition, PP2A inhibitor CIP2A is specifically overexpressed in numerous types of tumors, while is barely detectable in normal cells, making it a potential therapeutic target. CIP2A overexpression has been shown to correlate with poor prognosis in several cancer subtypes (Junttila et al., 2007). Until recently, it was unknown how exactly CIP2A suppresses the functions of PP2A. A recent study resolved the 3D structure of CIP2A (Wang et al., 2017) and showed that CIP2A forms homodimers, which interact with the PP2A B56 subunits leading to CIP2A stabilization. According to this model, CIP2A traps B56 proteins (B56α and B56γ and possibly other B56 subunits as well). Downregulation of CIP2A by metformin leads to reduced trapping of B56 proteins and, when combined with low glucose-induced B56δ upregulation, ultimately enhances recruitment of B56δ to the PP2A complex.

It has also been proposed that CIP2A interacts with the A subunit and impairs binding of B subunits to PP2A complexes (Junttila et al., 2007; Khanna et al., 2013). According to this model, it is possible that metformin-induced downregulation of CIP2A frees PP2A A and C subunits from the inhibitory interaction with CIP2A, which when combined with low glucose-induced B56δ upregulation, allows the formation of an active complex of PP2A A, C and B56δ subunits.

Downstream of the PP2A complex, our results establish a crucial role for GSK3β and MCL-1 in mediating the observed synergistic cytotoxicity. GSK3β has been shown previously to be a target of metformin (Gwak et al., 2017). Our results show a differential modulation of GSK3β by metformin alone as compared with the combination of metformin with low glucose. The specific GSK3β dephosphorylation by PP2A confirmed that the molecular signaling driven by the combination cannot simply be attributed to the sum of the events triggered by each of the two treatments individually.

(B) Percentage of cell death of control or B56δ-depleted HCT116 and HeLa cells cultured for 24 h in DMEM (replenished every 6 h) containing either 10 or 2.5 mM glucose in the absence or presence of Metformin (5 mM).

(C) Cell proliferation assessed by CellTiter-Glo assay of control or B56δ-depleted HCT116 and HeLa cells cultured in DMEM containing the indicated concentration of glucose and treated with increasing concentrations of metformin for 24 h.

(D) Immunoprecipitation analysis of PP2A Aα from cell lysates used in (A).

(E) Immunoblotting analysis of lysates-derived PP2A Aα-depleted HCT116 cells reconstituted with either an empty vector, or wild-type or S256F mutant PP2A Aα constructs cultured for 24 h in DMEM (replenished every 6 h) containing either 10 or 2.5 mM glucose in the absence or presence of Metformin (5 mM).

(F) Immunoblotting analysis of lysates derived from HCT116 cells overexpressing either vector or B56δ construct cultured in 10 mM glucose DMEM and treated for 24 h with either vehicle or metformin (5 mM).

(G) Percentage of cell death of HCT116 and HeLa cells overexpressing either vector or B56δ construct cultured in 10 mM glucose DMEM and treated for 24 h with the indicated concentrations of metformin. Results are representative of three biologically independent experiments.

Error bars in all the panels of this figure indicate SD. Average intensities of the bands from three biologically independent repeats normalized to loading control and expressed as fold change of the first band ± SD are presented under each lane. Student's t test was used for statistical analysis (n.s., non-significant). $^{n.s.}p > 0.05$, $^{*}p \leq 0.05$, $^{**}p \leq 0.01$, $^{***}p \leq 0.001$, $^{****}p \leq 0.0001$. See also Figure S7.

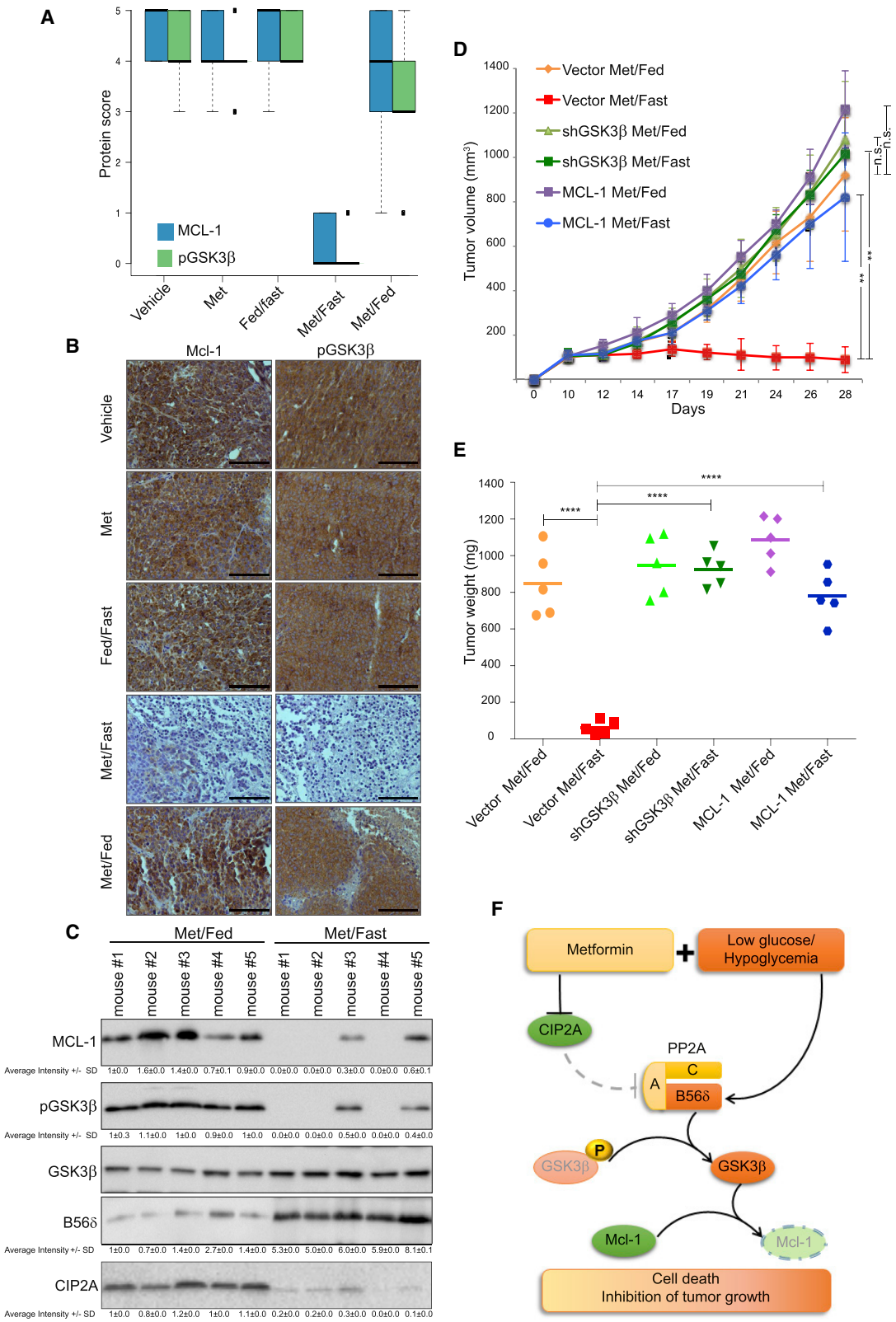


**Figure 8. Modulation of GSK3β-MCL-1 Axis Mediates Tumor Sensitization to Metformin Administered during Fasting-Induced Hypoglycemia**

(A and B) Quantification (A) and representative images (B) of immunohistochemical analysis of MCL-1 and phosphorylated GSK3β in tissue samples isolated from mice treated as in Figure 1. Scale bars, 100 μm. The boxplot displays the distribution of protein scores. The upper and lower whiskers indicate the maximal and

*(legend continued on next page)*

Besides the well-established anti-apoptotic functions of MCL-1, other tumor-promoting roles in autophagy and cellular bioenergetics are emerging (Elgendy, 2017; Elgendy et al., 2014, 2017; Elgendy and Minucci, 2015; Perciavalle et al., 2012). MCL-1 levels were slightly reduced by treatment with metformin alone, which may contribute to priming to apoptosis as MCL-1 overexpression completely abolished the very modest cytotoxicity of metformin.

While metformin may exhibit single-agent activity in some contexts, there is generally more interest in exploring its potential use in combinatorial therapy. The combination of metformin with IF or PP2A inducers may prove efficacious in targeting cancer cells and warrants further clinical evaluation. In addition, our results predict that the functional/genetic loss of PP2A will lead to loss of synergism in treatment, and suggest a potential strategy for stratification of patients.

## STAR★METHODS

Detailed methods are provided in the online version of this paper and include the following:

- KEY RESOURCES TABLE
- CONTACT FOR REAGENT AND RESOURCE SHARING
- EXPERIMENTAL MODEL AND SUBJECT DETAILS
  - Patient-Derived Cells
  - Xenograft Tumor Models
  - Cell Lines
- METHOD DETAILS
  - Immunoblotting
  - Lentiviral Transduction
  - Quantification of Cell Proliferation
  - Quantification of Cell Death
  - Lactate Production Assay
  - Oxygen Consumption Assay
  - Immunohistochemistry
  - Glucose Measurement in Tumors
  - Clonogenic Survival Assay
  - Quantitative Real-Time Polymerase Chain Reaction (qRT-PCR)
  - AMP/ATP Assay
- QUANTIFICATION AND STATISTICAL ANALYSIS

## SUPPLEMENTAL INFORMATION

Supplemental Information can be found online at https://doi.org/10.1016/j.ccell.2019.03.007.

## ACKNOWLEDGMENTS

We thank Dr Marco Giorgio (European Institute of Oncology, Milan) for help with the *in vivo* work, and Dr Russell Jones (McGill University, Montreal) for providing AMPK α1/α2 shRNA. M.E. has been awarded fellowships by AIRC, FUV, the Mahlke-Obermann Stiftung, and the European Union's Seventh Framework Programme/FP7 Marie Curie Actions Grant Agreement no. 609431/INDICAR–Interdisciplinary Cancer Research. B.B. received funding from AIRC (IG 12072) and from the Italian Ministery of Health (RRC-2014-2354553). V.J. was supported by F.W.O.-Flanders (G.0B01.16N). Work in the laboratory of S.M. is funded by AIRC. M.F. and S.M. received funding by Regione Lombardia (grant DIVA).

## AUTHOR CONTRIBUTIONS

Conceptualization, M.E. and S.M.; Methodology, M.E.; Contribution to Methodology, M.C., A.H., R.C., and J.W.; Writing, M.E. and S.M.; Resources, V.J. and W.W.; Discussion and Critical Comments, L.M., E.F., G.C., A.D., B.B., V.J., M.B., A.B., M.O., W.W., P.G.P., and M.F.; Supervision, S.M.

## DECLARATION OF INTERESTS

M.E., R.C., M.F., and S.M. are inventors on the patent application PCT/EP2018/063257 related to the subject matter of this study. The authors declare no other competing interests.

Received: January 2, 2018
Revised: January 5, 2019
Accepted: March 27, 2019
Published: April 25, 2019

## REFERENCES

Akinyeke, T., Matsumura, S., Wang, X., Wu, Y., Schalfer, E.D., Saxena, A., Yan, W., Logan, S.K., and Li, X. (2013). Metformin targets c-MYC oncogene to prevent prostate cancer. Carcinogenesis *34*, 2823–2832.

Bennecib, M., Gong, C.X., Grundke-Iqbal, I., and Iqbal, K. (2000). Role of protein phosphatase-2A and -1 in the regulation of GSK-3, cdk5 and cdc2 and the phosphorylation of tau in rat forebrain. FEBS Lett. *485*, 87–93.

Birsoy, K., Possemato, R., Lorbeer, F.K., Bayraktar, E.C., Thiru, P., Yucel, B., Wang, T., Chen, W.W., Clish, C.B., and Sabatini, D.M. (2014). Metabolic determinants of cancer cell sensitivity to glucose limitation and biguanides. Nature *508*, 108–112.

Bonanni, B., Puntoni, M., and Cazzaniga, M. (2012). Dual effect of metformin on breast cancer proliferation in a randomized presurgical trial. J. Clin. Oncol. *30*, 2593–2600.

Chien, W., Sun, Q.-Y., Lee, K.L., Ding, L.-W., Wuensche, P., Torres-Fernandez, L.A., Tan, S.Z., Tokatly, I., Zaiden, N., Poellinger, L., et al. (2015). Activation of protein phosphatase 2A tumor suppressor as potential treatment of pancreatic cancer. Mol. Oncol. *9*, 889–905.

Cohen, P., and Frame, S. (2001). The renaissance of GSK3. Nat. Rev. Mol. Cell Biol. *2*, 769–776.

minimal scores, respectively, excluding outliers, the boxes indicate the highest and lowest quartiles, the thick bars indicate the medians, and the dots indicate the outliers (more or less than 1.5 times the upper or lower quartile, respectively). In some cases, due to the homogeneous score among the tissue samples analyzed, quartiles overlap with the median values.

(C) Immunoblotting analysis of tumor lysates derived from mice treated as in Figure 1.

(D) *In vivo* growth of tumor xenografts in mice inoculated with control, GSk3β-depleted, or MCL-1-overexpressing HCT116 cells. On establishment of tumors, mice were kept on 24-h feeding/fasting cycles and treated with metformin (200 mg/kg) administered by oral gavage every 48 h either during feeding cycles (Met/Fed) or during fasting cycle (Met/fast). Error bars indicate SEM (n = 5 per group).

(E) Weight of tumors from (D), isolated at the end of the treatment. Horizontal bars indicate median tumor weight.

(F) Schematic representation of the molecular mechanism of targeting metabolic plasticity of tumor cells by low glucose-metformin combination. Average intensities of the bands from three biologically independent repeats normalized to loading control and expressed as fold change of the first band ± SD are presented under each lane.

Student's t test was used for statistical analysis (n.s., non-significant). $^{n.s.}p > 0.05$, $^{**}p \leq 0.01$, $^{****}p \leq 0.0001$. See also Figure S8.

DeBerardinis, R.J., and Chandel, N.S. (2016). Fundamentals of cancer metabolism. Sci. Adv. *2*, e1600200.

DeCensi, A., Puntoni, M., Gandini, S., Guerrieri-Gonzaga, A., Johansson, H.A., Cazzaniga, M., Pruneri, G., Serrano, D., Schwab, M., Hofmann, U., et al. (2014). Differential effects of metformin on breast cancer proliferation according to markers of insulin resistance and tumor subtype in a randomized presurgical trial. Breast Cancer Res. Treat. *148*, 81–90.

Dykens, J.A., Jamieson, J., Marroquin, L., Nadanaciva, S., Billis, P.A., and Will, Y. (2008). Biguanide-induced mitochondrial dysfunction yields increased lactate production and cytotoxicity of aerobically-poised HepG2 cells and human hepatocytes in vitro. Toxicol. Appl. Pharmacol. *233*, 203–210.

Elgendy, M. (2017). The yin yang of sunitinib: one drug, two doses, and multiple outcomes. Mol. Cell. Oncol. *4*, e1285385.

Elgendy, M., and Minucci, S. (2015). A novel autophagy-independent, oncosuppressive function of BECN1: degradation of MCL1. Autophagy *11*, 581–582.

Elgendy, M., Ciro, M., Abdel-Aziz, A.K., Belmonte, G., Dal Zuffo, R., Mercurio, C., Miracco, C., Lanfrancone, L., Foiani, M., and Minucci, S. (2014). Beclin 1 restrains tumorigenesis through Mcl-1 destabilization in an autophagy-independent reciprocal manner. Nat. Commun. *5*, 5637.

Elgendy, M., Abdel-Aziz, A.K., Renne, S.L., Bornaghi, V., Procopio, G., Colecchia, M., Kanesvaran, R., Toh, C.K., Bossi, D., Pallavicini, I., et al. (2017). Dual modulation of MCL-1 and mTOR determines the response to sunitinib. J. Clin. Invest. *127*, 153–168.

Ferrari, E., Bruhn, C., Peretti, M., Cassani, C., Carotenuto, W.V., Elgendy, M., Shubassi, G., Lucca, C., Bermejo, R., Varasi, M., et al. (2017). PP2A controls genome integrity by integrating nutrient-sensing and metabolic pathways with the DNA damage response. Mol. Cell *67*, 266–281.e4.

Gutierrez, A., Pan, L., Groen, R.W.J., Baleydier, F., Kentsis, A., Marineau, J., Grebliunaite, R., Kozakewich, E., Reed, C., Pflumio, F., et al. (2014). Phenothiazines induce PP2A-mediated apoptosis in T cell acute lymphoblastic leukemia. J. Clin. Invest. *124*, 644–655.

Gwak, H., Kim, Y., An, H., Dhanasekaran, D.N., and Song, Y.S. (2017). Metformin induces degradation of cyclin D1 via AMPK/GSK3β axis in ovarian cancer. Mol. Carcinog. *56*, 349–358.

Haesen, D., Asbagh, L.A., Derua, R., Hubert, A., Schrauwen, S., Hoorne, Y., Amant, F., Waelkens, E., Sablina, A., and Janssens, V. (2016). Recurrent PPP2R1A mutations in uterine cancer act through a dominant-negative mechanism to promote malignant cell growth. Cancer Res. *76*, 5719–5731.

Hao, W., Chang, C.P.B., Tsao, C.C., and Xu, J. (2010). Oligomycin-induced bioenergetic adaptation in cancer cells with heterogeneous bioenergetic organization. J. Biol. Chem. *285*, 12647–12654.

Havas, K.M., Milchevskaya, V., Radic, K., Alladin, A., Kafkia, E., Garcia, M., Stolte, J., Klaus, B., Rotmensz, N., Gibson, T.J., et al. (2017). Metabolic shifts in residual breast cancer drive tumor recurrence. J. Clin. Invest. *127*, 2091–2105.

Janssens, V., Goris, J., and Van Hoof, C. (2005). PP2A: the expected tumor suppressor. Curr. Opin. Genet. Dev. *15*, 34–41.

Jose, C., Bellance, N., and Rossignol, R. (2011). Choosing between glycolysis and oxidative phosphorylation: a tumor's dilemma? Biochim. Biophys. Acta *1807*, 552–561.

Junttila, M.R., Puustinen, P., Niemelä, M., Ahola, R., Arnold, H., Böttzauw, T., Ala-aho, R., Nielsen, C., Ivaska, J., Taya, Y., et al. (2007). CIP2A inhibits PP2A in human malignancies. Cell *130*, 51–62.

Kalender, A., Selvaraj, A., Kim, S.Y., Gulati, P., Brûlé, S., Viollet, B., Kemp, B.E., Bardeesy, N., Dennis, P., Schlager, J.J., et al. (2010). Metformin, independent of AMPK, inhibits mTORC1 in a rag GTPase-dependent manner. Cell Metab. *11*, 390–401.

Kim, S.M., Roy, S.G., Chen, B., Nguyen, T.M., McMonigle, R.J., McCracken, A.N., Zhang, Y., Kofuji, S., Hou, J., Selwan, E., et al. (2016). Targeting cancer metabolism by simultaneously disrupting parallel nutrient access pathways. J. Clin. Invest. *126*, 4088–4102.

Lambrecht, C., Libbrecht, L., Sagaert, X., Pauwels, P., Hoorne, Y., Crowther, J., Louis, J.V., Sents, W., Sablina, A., and Janssens, V. (2018). Loss of protein phosphatase 2A regulatory subunit B56δ promotes spontaneous tumorigenesis in vivo. Oncogene *37*, 544–552.

Lee, C., and Longo, V.D. (2011). Fasting vs dietary restriction in cellular protection and cancer treatment: from model organisms to patients. Oncogene *30*, 3305–3316.

Lee, C., Raffaghello, L., Brandhorst, S., Safdie, F.M., Bianchi, G., Martin-Montalvo, A., Pistoia, V., Wei, M., Hwang, S., Merlino, A., et al. (2012). Fasting cycles retard growth of tumors and sensitize a range of cancer cell types to chemotherapy. Sci. Transl. Med. *4*, 124ra27.

Longo, V.D., and Mattson, M.P. (2014). Fasting: molecular mechanisms and clinical applications. Cell Metab. *19*, 181–192.

Martin, M.J., Hayward, R., Viros, A., and Marais, R. (2012). Metformin accelerates the growth of BRAFV600E-driven melanoma by upregulating VEGF-A. Cancer Discov. *2*, 344–355.

Maurer, U., Charvet, C., Wagman, A.S., Dejardin, E., and Green, D.R. (2006). Glycogen synthase kinase-3 regulates mitochondrial outer membrane permeabilization and apoptosis by destabilization of MCL-1. Mol. Cell *21*, 749–760.

Mitra, A., Menezes, M.E., Pannell, L.K., Mulekar, M.S., Honkanen, R.E., Shevde, L.A., and Samant, R.S. (2012). DNAJB6 chaperones PP2A mediated dephosphorylation of GSK3β to downregulate β-catenin transcription target, osteopontin. Oncogene *31*, 4472–4483.

Mumby, M. (2007). PP2A: unveiling a reluctant tumor suppressor. Cell *130*, 21–24.

Obre, E., and Rossignol, R. (2015). Emerging concepts in bioenergetics and cancer research: metabolic flexibility, coupling, symbiosis, switch, oxidative tumors, metabolic remodeling, signaling and bioenergetic therapy. Int. J. Biochem. Cell Biol. *59*, 167–181.

Perciavalle, R.M., Stewart, D.P., Koss, B., Lynch, J., Milasta, S., Bathina, M., Temirov, J., Cleland, M.M., Pelletier, S., Schuetz, J.D., et al. (2012). Anti-apoptotic MCL-1 localizes to the mitochondrial matrix and couples mitochondrial fusion to respiration. Nat. Cell Biol. *14*, 575–583.

Pollak, M.N. (2012). Investigating metformin for cancer prevention and treatment: the end of the beginning. Cancer Discov. *2*, 778–790.

Pusapati, R.V., Daemen, A., Wilson, C., Sandoval, W., Gao, M., Haley, B., Baudy, A.R., Hatzivassiliou, G., Evangelista, M., and Settleman, J. (2016). mTORC1-dependent metabolic reprogramming underlies escape from glycolysis addiction in cancer cells. Cancer Cell *29*, 548–562.

Qiu, X., Brown, K., Hirschey, M.D., Verdin, E., and Chen, D. (2010). Calorie restriction reduces oxidative stress by SIRT3-mediated SOD2 activation. Cell Metab. *12*, 662–667.

Quinn, B.J., Dallos, M., Kitagawa, H., Kunnumakkara, A.B., Memmott, R.M., Hollander, M.C., Gills, J.J., and Dennis, P.A. (2013). Inhibition of lung tumorigenesis by metformin is associated with decreased plasma IGF-I and diminished receptor tyrosine kinase signaling. Cancer Prev. Res. (Phila.) *6*, 801–810.

Raffaghello, L., Lee, C., Safdie, F.M., Wei, M., Madia, F., Bianchi, G., and Longo, V.D. (2008). Starvation-dependent differential stress resistance protects normal but not cancer cells against high-dose chemotherapy. Proc. Natl. Acad. Sci. U S A *105*, 8215–8220.

Safdie, F.M., Dorff, T., Quinn, D., Fontana, L., Wei, M., Lee, C., Cohen, P., and Longo, V.D. (2009). Fasting and cancer treatment in humans: a case series report. Aging *1*, 988–1007.

Sangodkar, J., Perl, A., Tohme, R., Kiselar, J., Kastrinsky, D.B., Zaware, N., Izadmehr, S., Mazhar, S., Wiredja, D.D., O'Connor, C.M., et al. (2017). Activation of tumor suppressor protein PP2A inhibits KRAS-driven tumor growth. J. Clin. Invest. *127*, 2081–2090.

Stine, Z.E., Walton, Z.E., Altman, B.J., Hsieh, A.L., and Dang, C.V. (2015). MYC, metabolism, and cancer. Cancer Discov. *5*, 1024–1039.

Um, J.H., Yang, S., Yamazaki, S., Kang, H., Viollet, B., Foretz, M., and Chung, J.H. (2007). Activation of 5′-AMP-activated kinase with diabetes drug metformin induces casein kinase Iepsilon (CKIepsilon)-dependent degradation of clock protein mPer2. J. Biol. Chem. *282*, 20794–20798.

Vander Heiden, M.G. (2011). Targeting cancer metabolism: a therapeutic window opens. Nat. Rev. Drug Discov. *10*, 671–684.

Wang, R., Xia, L., Gabrilove, J., Waxman, S., and Jing, Y. (2012). Downregulation of Mcl-1 through GSK-3β activation contributes to arsenic trioxide-induced apoptosis in acute myeloid leukemia cells. Leukemia *27*, 315–324.

Wang, J., Okkeri, J., Pavic, K., Wang, Z., Kauko, O., Halonen, T., Sarek, G., Ojala, P.M., Rao, Z., Xu, W., et al. (2017). Oncoprotein CIP2A is stabilized via interaction with tumor suppressor PP2A/B56. EMBO Rep. *18*, 437–450.

Weckwerth, W., Wenzel, K., and Fiehn, O. (2004). Process for the integrated extraction, identification and quantification of metabolites, proteins and RNA to reveal their co-regulation in biochemical networks. Proteomics *4*, 78–83.

Zhou, G., Myers, R., Li, Y., Chen, Y., Shen, X., Fenyk-Melody, J., Wu, M., Ventre, J., Doebber, T., Fujii, N., et al. (2001). Role of AMP-activated protein kinase in mechanism of metformin action. J. Clin. Invest. *108*, 1167–1174.

Zhuang, Y., Chan, D.K., Haugrud, A.B., and Miskimins, W.K. (2014). Mechanisms by which low glucose enhances the cytotoxicity of metformin to cancer cells both in vitro and in vivo. PLoS One *9*, e108444.

## STAR★METHODS

### KEY RESOURCES TABLE

| REAGENT or RESOURCE | SOURCE | IDENTIFIER |
|---|---|---|
| Antibodies | | |
| phospho-AMPKα (Thr172) (40H9) Rabbit mAb | Cell Signaling Technology | Cat. #: 2535 RRID:AB_331250 |
| AMPKα (F6) Mouse mAb | Cell Signaling Technology | Cat. #: 2793 RRID: N/A |
| Phospho-Acetyl-CoA Carboxylase (Ser79) Antibody | Cell Signaling Technology | Cat. #: 3661 RRID:AB_330337 |
| Acetyl-CoA Carboxylase (C83B10) Rabbit mAb | Cell Signaling Technology | Cat. #: 3676 RRID:AB_2219397 |
| Phospho-GSK3β (Ser9) (5B3) Rabbit mAb | Cell Signaling Technology | Cat. #: 9323 RRID: N/A |
| GSK3β (D5C5Z) XP® Rabbit mAb | Cell Signaling Technology | Cat. #: 12456 RRID: N/A |
| Phospho-p44/42 MAPK (ERK1/2) Rabbit pAb | Cell Signaling Technology | Cat #9101; RRID:AB_331646 |
| p44/42 MAPK (ERK1/2) Rabbit pAb | Cell Signaling Technology | Cat #9102; RRID:AB_330744 |
| Phospho-GSK3α (Ser21) (D1G2) Rabbit mAb | Cell Signaling Technology | Cat. #: 8452 RRID: N/A |
| GSK3α Antibody | Cell Signaling Technology | Cat. #: 9338 RRID: N/A |
| Phospho-Akt (Ser473) Rabbit pAb | Cell Signaling Technology | Cat #9271; RRID:AB_329825 |
| Akt Rabbit pAb | Cell Signaling Technology | Cat #9272; RRID:AB_329827 |
| Cleaved Caspase-3 (Asp175) Antibody | Cell Signaling Technology | Cat. #: 9661 RRID: N/A |
| Cleaved Caspase-7 (Asp198) Antibody | Cell Signaling Technology | Cat. #: # 9491, RRID:AB_2068144 |
| Anti-Vinculin antibody, Mouse mAb | Sigma Aldrich (now Merck) | Cat# V4505, RRID:AB_477617 |
| PP2A-Aα pAb (clone C-20) | Santa Cruz Biotechnology | Cat. #: sc-6112 RRID: N/A |
| MCL-1 pAb (clone S-19) | Santa Cruz Biotechnology | Cat. #: sc-819 RRID:AB_2144105 |
| PP2A-B56δ pAb (clone C-15) | Santa Cruz Biotechnology | Cat. #: sc-107956 RRID: N/A |
| CIP2A Antibody (HL1925) | Santa Cruz Biotechnology | Cat. #: sc-80662 RRID:AB_2130800 |
| Anti-c-Myc antibody [Y69] | Abcam | Cat. #: ab32072 RRID: N/A |
| Purified Mouse Anti-PP2A Catalytic α Clone 46 | BD Biosciences | Cat. #: 610555 RRID: N/A |
| Purified Mouse Anti-BCL-2 | BD Biosciences | Cat# 551097, RRID:AB_394044 |
| Purified Mouse Anti-BCL-xL | BD Biosciences | Cat. #: 610747, RRID:AB_398070 |
| Mouse Anti-Cleaved PARP (Asp214) | BD Biosciences | Cat# 552596, RRID:AB_394437 |
| Chemicals, Peptides, and Recombinant Proteins | | |
| Metformin | Sigma Aldrich | Cat. #: PHR1084 |
| GSK3β inhibitor xii (TWS119) | Selleck Chem. | Cat. #: S1590 |
| GSK3β inhibitor xii (TWS119) | Selleck Chem. | Cat. #: S1590 |
| GSK3β inhibitor viii (AR-A014418) | Selleck Chem. | Cat. #: S7435 |
| U0126-EtOH | Selleck Chem. | Cat. #: S1102 |
| PD98059 | Selleck Chem. | Cat. #: S1177 |
| SP600125 | Selleck Chem. | Cat. #:S1460 |
| SB202190 (FHPI) | Selleck Chem. | Cat. #:S1077 |
| MG132 | Selleck Chem. | Cat. # S2619 |
| Z-VAD-FMK | Selleck Chem. | Cat. # S7023 |
| Z-DEVD-FMK | Selleck Chem. | Cat. # S7312 |
| Epoxomicin | Sigma Aldrich | Cat. # E3652 |
| 2-Deoxy-D-glucose | Sigma Aldrich | Cat. # D8375 |
| Perphenazine | Sigma Aldrich | Cat. # P6402- |
| Glucose solution | Gibco (Now Thermo Fischer) | Cat. # A24940-01 |
| Critical Commercial Assays | | |
| CellTitreGlo | Promega | Cat. # G7570 |
| Lactate Assay Kit | Sigma Aldrich | Cat. # MAK064-1KT |
| Oxygen Consumption Rate Assay Kit (MitoXpress® Xtra HS Method). | Cayman Chemical | Cat. # 600800 |

(*Continued on next page*)

*Continued*

| REAGENT or RESOURCE | SOURCE | IDENTIFIER |
|---|---|---|
| Experimental Models: Cell Lines | | |
| MCF7 | ATCC (the American Type Culture Collection) | |
| A2780 | ECACC (The European Collection of Authenticated Cell Cultures) | |
| COLO-704 | DSMZ (Deutsche Sammlung von Mikroorganismen und Zellkulturen GmbH) | |
| A375 | IZSLER (Istituto Zooprofilattico Sperimentale della Lombardia e dell'emilia Romagna) | |
| SK MEL 28 | ICLC (IRCCS AOU San Martino - IST Istituto Nazionale per la Ricerca sul Cancro) | |
| PLC-PRF-5 | ATCC (the American Type Culture Collection) | |
| IGR-1 | DSMZ (Deutsche Sammlung von Mikroorganismen und Zellkulturen GmbH) | |
| G-361 | ICLC (IRCCS AOU San Martino - IST Istituto Nazionale per la Ricerca sul Cancro) | |
| COLO 858 | ICLC (IRCCS AOU San Martino - IST Istituto Nazionale per la Ricerca sul Cancro) | |
| C32 | IZSLER (Istituto Zooprofilattico Sperimentale della Lombardia e dell'emilia Romagna) | |
| MALME 3M | ATCC (the American Type Culture Collection) | |
| IPC-298 | DSMZ (Deutsche Sammlung von Mikroorganismen und Zellkulturen GmbH) | |
| SK-MEL30 | DSMZ (Deutsche Sammlung von Mikroorganismen und Zellkulturen GmbH) | |
| SK-MEL3 | DSMZ (Deutsche Sammlung von Mikroorganismen und Zellkulturen GmbH) | |
| WM266-4 | ECACC (The European Collection of Authenticated Cell Cultures) | |
| MEWO | ICLC (IRCCS AOU San Martino - IST Istituto Nazionale per la Ricerca sul Cancro) | |
| IGR-37 | DSMZ (Deutsche Sammlung von Mikroorganismen und Zellkulturen GmbH) | |
| RPMI 7951 | DSMZ (Deutsche Sammlung von Mikroorganismen und Zellkulturen GmbH) | |
| COLO-679 | DSMZ (Deutsche Sammlung von Mikroorganismen und Zellkulturen GmbH) | |
| GaLa1949 | This paper | N/A |
| LuCa1973 | This paper | N/A |
| Experimental Models: Organisms/Strains | | |
| CD1 nude mice (CD1-Foxn1nu) | Charles River Laboratories | N/A |
| Oligonucleotides | | |
| Primers for PPP2R5D: Forward: GGCCGAGATGTCCTATAAACTG | This paper | N/A |
| Primers for KIAA1524: Forward : CCATATGCTCACTCAGATGATGT | This paper | N/A |

(*Continued on next page*)

*Continued*

| REAGENT or RESOURCE | SOURCE | IDENTIFIER |
|---|---|---|
| Recombinant DNA | | |
| pLKO.1 scrambled shRNA<br>Target sequence: GTGGACTCTTGAAAGTACTAT | | |
| pLKO.1 human PPP2R1A shRNA #1<br>Target sequence: TTGCCAATGTCCGCTTCAATGC | Sigma Aldrich | Clone ID: NM_014225.3-1714s21c1 |
| pLKO.1 human PPP2R1A shRNA #2<br>Target sequence: CTACGCTCTTCTGCATCAATGC | Sigma Aldrich | Clone ID: NM_014225.3-1615s21c1 |
| pLKO.1 human PPP2CA shRNA<br>Target sequence: GGCAAATCACCAGATACAAATC | Sigma Aldrich | Clone ID: NM_002715.2-615s21c1 |
| pLKO.1 human PPP2R5D shRNA #1<br>Target sequence: AGTCTGACTGAGCCGGTAATTC | Sigma Aldrich | Clone ID: NM_006245.2-1152s21c1 |
| pLKO.1 human PPP2R5D shRNA #2<br>Target sequence: CACATCTCCAGCTCGTGTATGC | Sigma Aldrich | Clone ID: NM_006245.2-709s21c1 |
| pLKO.1 human KIAA1524 shRNA<br>Target sequence: TGCGGCACTTGGAGGTAATTTC | Sigma Aldrich | Clone ID: NM_020890.2-358s21c1 |
| pLKO.1 human GSK3B shRNA #1<br>Target sequence: GCTGAGCTGTTACTAGGACAA | Sigma Aldrich | Clone ID: NM_002093.2-974s1c1 |
| pLKO.1 human GSK3B shRNA #2<br>Target sequence: CACTGGTCACGTTTGGAAAGA | Sigma Aldrich | Clone ID: NM_002093.x-1596s1c1 |
| Software and Algorithms | | |
| ImageJ | https://imagej.nih.gov/ij/ | |
| Compusyn | www.combosyn.com/ | |
| Image Lab | BioRad | |

## CONTACT FOR REAGENT AND RESOURCE SHARING

Further information and requests for reagents may be directed to, and will be fulfilled by the Lead Contact Saverio Minucci (saverio.minucci@ieo.it).

## EXPERIMENTAL MODEL AND SUBJECT DETAILS

### Patient-Derived Cells

Establishment of primary cells GaLa1949 and LuCa1970 from metastatic melanomas was previously described in (Elgendy et al., 2014). Briefly, tumor specimens from patients were dissected in Petri dishes containing RPMI 1640 + 10% FCS into small pieces with a scalpel. Cell suspension was filtered through sterile gauze to eliminate macroscopic debris. Following 45-min incubation at room temperature on a magnetic shaker, cell suspension was filtered through sterile gauze to remove debris. Cell suspension was recovered from the supernatant by centrifugation and extensively washed in RPMI 1640 + 10% FCS. Cells were grown in DMEM + 10% FBS and were periodically characterized by immunohistochemistry staining with S100, MelanA and HMB45 antibodies at various passages during the time they are kept in culture.

### Xenograft Tumor Models

CD1 nude mice received single subcutaneous flank injections of $5\times10^6$ HCT116 cells or melanoma cells or $1\times10^5$ patient-derived melanoma cells suspended in 200 μl saline. After the tumors were established, mice were randomized in different groups. Mice were kept on the feeding/fasting protocols. Fasting cycles were achieved by complete removal of food while allowing free access to water for 24 hr from 6 pm to 6 pm of the following day when food was re-supplied *ad libitum*. Metformin, at 200 mg/kg dissolved in water, was administered every 48 hr at 9 am via oral gavage. Tumor growth was monitored by bi-dimensional measurements using a caliper. Tumor volume was calculated as (length x width x width)/2. Note that nude mice show a strain-specific decline in glucose levels upon fasting, of a higher degree as compared to other commonly used mouse strains (such as C57B6: data not shown). Experiments have been done in accordance with the Italian Laws (D.L.vo 116/92 and following additions), which enforces EU 86/609 Directive (Council Directive 86/609/EEC of 24 November 1986 on the approximation of laws, regulations and administrative provisions of the Member States regarding the protection of animals used for experimental and other scientific purposes). Mice have

been housed accordingly to the guidelines set out in Commission Recommendation 2007/526/EC - June 18, 2007 on guidelines for the accommodation and care of animals used for experimental and other scientific purposes. The protocol was approved by the Italian Ministry of Health (Authorization 1075/2016-PR).

### Cell Lines

HCT116 and HeLa cell lines were grown in Dulbecco's modified Eagle's medium (DMEM) supplemented with 10% fetal bovine serum and 2 mM L-glutamine unless otherwise indicated. Other cell lines were grown in RPMI medium supplemented with 10% fetal bovine serum and 2 mM L-glutamine unless otherwise indicated. For starvation experiments, cells were washed three times with PBS pH 7.2 and then incubated in the indicated starvation conditions. All cultures were maintained in a humidified tissue culture incubator at 37°C in 5% CO2.

## METHOD DETAILS

### Immunoblotting

Whole cell lysates were prepared by directly lysing cells growing in culturing dishes or collected cell pellets in lysis buffer (40 mM Hepes pH 7.5, 120 mM NaCl, 1 mM EDTA, 10 mM pyrophosphate, 10 mM glycerophosphate, 50 mM NaF, 0.5 mM orthovanadate, and EDTA-free protease inhibitors (Roche) containing 0.3% CHAPS). Lysates were prepared from frozen tumors using GentleMACS dissociator. Lysates were cleared by centrifugation at 13000 g for 15 min. at 4°C, quantified using BioRad DC protein assay reagent followed by mixing 1:1 with 4% SDS, 100 mM Tris.Cl pH 6.8, 20% glycerol, 0.1% bromophenol blue and 5% β-mercaptoethanol added immediately before use and heating at 94°C for 7 min. Equal amounts of proteins were then subjected to 8-15% SDS-PAGE gels. Gels were run at 100 V (stacking gel) / 150 V (separation gel) on Protean III apparatus (BioRad). Gels were transferred onto nitrocellulose membranes and probed with the appropriate primary antibody, followed by the corresponding secondary antibodies diluted 1:5000-10000. The proteins were visualized by enhanced chemiluminescence (ECL) using ChemiDoc apparatus (BioRad) according to the manufacturer's instructions. Optical intensity of the bands was quantified using ImageJ software. Average intensities of the bands from three biologically-independent repeats expressed as fold change of the first band +/- SD are presented under each lane. Statistical significance of change in intensity was assessed against the first band unless otherwise indicated under the blot. Student's t test was used for statistical analysis. n.s. (non-significant): $P > 0.05$, *: $P \leq 0.05$, **: $P \leq 0.01$, ***: $P \leq 0.001$, ****: $P \leq 0.0001$.

### Lentiviral Transduction

shRNA pLKO.1 lentiviral constructs were purchased from Sigma Aldrich. The pLKO.1 vectors and package plasmids were co-transfected into packaging HEK293T cells and the viral supernatants were collected, supplemented with polybrene (8 μg/mL) and used to infect target cells in four cycles of transduction, 2-hr each over two consecutive days.

### Quantification of Cell Proliferation

CellTiterGlo Luminescent Cell Viability Assay (Promega) was used according to manufacturer's protocol. Briefly, cells were plated in 96 well plates, treated 24 hr later with different doses of drugs in total volume of 100 μl. 24 hr later, 100 μl of CellTiter Glo reagent was added to the cells and incubated for 15 min at 37°C and luminescence was measured using a Promega plate reader.

### Quantification of Cell Death

Cell viability was assessed by trypan blue exclusion assay counting 300 cells from each condition. Additionally, cells were harvested by trypsinization, washed in PBS (pH 7.2), and then stained with propidium iodide (10 mg/ml) added immediately prior to analysis. Cell fluorescence was then measured on a flow cytometer (FACSCalibur; Becton Dickinson, CA) and analyzed using CellQuest software.

### Lactate Production Assay

Lactate production was measured using Lactate Assay Kit (Sigma Aldrich) according to manufacturer's instructions. Briefly, cells from different conditions were homogenized in 4 volumes of the Lactate Assay Buffer. Samples were centrifuged at 13,000 g for 10 min to remove insoluble material and de-proteinized with a 10 kDa MWCO spin filter to remove lactate dehydrogenase. Samples were brought up to final volume of 50 μL/well with Lactate Assay Buffer and mixed with 50 μL of the Master Reaction Mix (46 μL Lactate Assay Buffer + 2 μL Lactate Enzyme Mix + 2 μL Lactate Probe). The reaction mix was incubated for 30 min at room temperature in dark. And the absorbance was measured at 570 nm.

### Oxygen Consumption Assay

Oxygen Consumption Rate was measured using Oxygen Consumption Rate Assay Kit (MitoXpress® Xtra HS Method, Cayman Chemical) according to manufacturer's instructions. Briefly, 10 μl of culture medium from different conditions were added to of 10 μl phosphorescent oxygen probe solution and the mix was gently overlaid with 100 μl of pre-warmed HS mineral oil. Fluorescence kinetics of samples, blanks and controls were measured at excitation wavelength of 380 and emission of 620 nm.

### Immunohistochemistry

Formalin fixed paraffin embedded samples of tumors were cut 5 μm thick on polarized glass; unmasking for both antigen was made with Citrate for 30' at 99°C; anti-MCL1 and anti-pGSK3β antibodies were used at 1:200 and 1:50 concentration respectively for 2 hr. LSAB 2 System-AP (DAKO) and Vulcan Fast Red Chromogen Kit 2 (Biocare Medical) were used as visualization system according to company working procedure. After hematoxilin and eosin review, the positivity of tumor cells was scored using a scoring system evaluating the staining pattern (homogeneous or heterogeneous scoring respectively 0,1), the intensity of staining in the most reactive area (absent/weak/moderate/strong scoring respectively 0, 1, 2 or 3) and the percentage of most reactive cells/total cancer cells (≤10%; <10% but ≤50%; and >50% scoring respectively 0, 1 or 2).

### Glucose Measurement in Tumors

Glucose concentration was determined by gas chromatography (GC) coupled to a time of flight (TOF) mass spectrometer (MS). Extraction and measurement were conducted according to a previously published protocol with some modifications (Weckwerth et al., 2004). In brief, homogenized tissue was extracted twice with a mixture of methanol, chloroform and water (5/2/1, v/v/v), with a subsequent phase separation, initiated by the addition of water. An additional extraction step with 80 % ethanol, in which the samples were heated to 80°C for 30 min, was conducted and the ethanol extract was combined with the polar phase of the previous extraction. The combined extract was dried using a vacuum concentrator (ScanVac, LaboGene). To prepare the samples for GC-MS analysis, derivatization using methoximation with Methoxyamine hydrochloride in pyridine (90 min at 30°C) and silylation by N-Methyl-N-(trimethylsilyl) trifluoroacetamide (30 min at 37°C) was conducted. The Instrument used for analysis was an Agilent 6890 gas chromatograph (Agilent Technologies®, Santa Clara, USA) with an Agilent HP-5Ms column (inner diameter: 0.25 mm, length: 30 m, film: 0.25 μm) coupled to a LECO Pegasus® GCxGC-TOF mass spectrometer (LECO Corporation, St. Joseph, USA). Peak deconvolution and integration was conducted in the software LECO Chromatof®. Glucose was identified by measuring purified external standards and peak areas were normalized to internal standards (Pentaerythritol and Phenyl β-D-glucopyranoside, both Sigma-Aldrich) and tissue fresh weight.

### Clonogenic Survival Assay

HCT116 cells transduced with the indicated constructs were plated at 5000 cells per well in 6-well plates and cultured in medium containing either 10 mM or 2.5 mM glucose in the absence or presence of metformin (5 mM), for 2 more weeks. Colonies were then stained with 0.5% crystal violet in 20% methanol and washed three times with PBS pH 7.2. Pictures of the plates were taken using Canon digital camera. Surface area coverage was quantified using ImageJ software.

### Quantitative Real-Time Polymerase Chain Reaction (qRT-PCR)

RNA was extracted using Qiagen RNA extraction kit according to manufacturer's protocol, converted to cDNA using M-MLV Reverse transcriptase (RNase H Minus, Point mutant) and random primers (Promega, Madison, WI, USA). qRT-PCR was conducted using SensiFast SYBR green fluorescent nucleic acid stain (Bioline, Alexandria, Australia). Sequence of primers was as follow:

### AMP/ATP Assay

Intracellular ATP and AMP concentrations were determined with the ATP/ADP/AMP Assay kit (Biomedical Research Service & Clinical Application, Buffalo, NY) according to the manufacturer's instruction. The luciferase bioluminescence was measured using a Tecan Infinite M200 luminometer.

## QUANTIFICATION AND STATISTICAL ANALYSIS

Student's t test was used to test the significance of differences in different experimental conditions. Multiple linear regression analysis was used to test the correlation between tumor growth (assessed by tumor weight) and intra-tumor glucose levels. Chou-Talalay statistical analysis method using Compusyn software was used to test the synergism between metformin treatment and low glucose/PPZ.